

REGULARIZATION OF THE BACKWARDS
KURAMOTO-SIVASHINSKY EQUATION

By
Jonathan Gustafsson

SUBMITTED IN PARTIAL FULFILLMENT OF THE
REQUIREMENTS FOR THE DEGREE OF
MASTER OF SCIENCE
AT
MCMASTER UNIVERSITY
HAMILTON, ONTARIO
SEPTEMBER 2007

MCMASTER UNIVERSITY

DEGREE: Master of Science, 2007

DEPARTMENT: School of Computational Engineering and Science,
Hamilton, Ontario

UNIVERSITY: McMaster University

TITLE: Regularization of the Backwards Kuramoto–Sivashinsky
Equation

AUTHOR: Jonathan Gustafsson, M. Sc. (Chalmers University)

SUPERVISOR: Dr. Bartosz Protas

PAGES: v, 76

To Nasim Shahbazian

Abstract

We are interested in backward-in-time solution techniques for evolutionary PDE problems arising in fluid mechanics. In addition to their intrinsic interest, such techniques have applications in recently proposed retrograde data assimilation. As our model system we consider the terminal value problem for the Kuramoto-Sivashinsky equation in a 1D periodic domain. The Kuramoto-Sivashinsky equation, proposed as a model for interfacial and combustion phenomena, is often also adopted as a toy model for hydrodynamic turbulence because of its multiscale and chaotic dynamics. Such backward problems are typical examples of ill-posed problems, where any disturbances are amplified exponentially during the backward march. Hence, regularization is required to solve such problems efficiently in practice. We consider regularization approaches in which the original ill-posed problem is approximated with a less ill-posed problem, which is achieved by adding a regularization term to the original equation. While such techniques are relatively well-understood for linear problems, it is still unclear what effect these techniques may have in the nonlinear setting. In addition to considering regularization terms with fixed magnitudes, we also explore a novel approach in which these magnitudes are adapted dynamically using simple concepts from the Control Theory.

Table of Contents

Table of Contents	iv
1 Introduction	2
1.1 Motivation	2
1.2 Regularization via solution of a less ill-posed problem	3
1.3 Structure of the thesis	4
2 Kuramoto–Sivashinsky Equation (KSE)	6
2.1 Rescaling the Kuramoto–Sivashinsky equation	8
2.2 Kuramoto–Sivashinsky equation in Fourier space	10
2.3 Form of the energy function spectrum	10
3 Numerical solution of the Kuramoto–Sivashinsky equation	14
4 Analogies between the TVP for the heat equation and the KSE	18
5 Regularization of the terminal value problem	21
5.1 General remarks	21
5.2 Regularization techniques	24
5.2.1 Hyperviscous regularization	25
5.2.2 Pseudo-parabolic regularization	25
5.3 Spectrum change due to regularization	26
5.3.1 The low wavenumber part of the spectrum	26
5.3.2 The high wavenumber part of spectrum	29
5.4 Energy, L_2 norm	31
5.4.1 Energy equation for hyperviscous regularization technique	31
5.4.2 Energy equation for the pseudo-parabolic technique	32
5.5 H^{-1} norm	32
5.5.1 Equation for H^{-1} norm for hyperviscous regularization technique	34
5.5.2 Equation for H^{-1} norm for pseudo-parabolic technique	34
5.6 Adaptive adjustment of the magnitudes of the regularization terms	34

5.6.1	Instantaneous adaptation	35
5.6.2	P -regulator	37
5.6.3	PD -regulator	37
5.6.4	Comparison to different adaptive schemes	37
6	Results of the regularization algorithms	39
6.1	Hyperviscous regularization	41
6.1.1	Regularization of the linearized Kuramoto–Sivashinsky equation . .	41
6.1.2	Instantaneous adaptation	47
6.1.3	L_2 norm with the P -regulator	47
6.1.4	L_2 norm with the PD -regulator	50
6.1.5	H^{-1} norm with P -regulator	53
6.2	Pseudo-parabolic regularization	56
6.2.1	Regularization of the linearized Kuramoto–Sivashinsky equation . .	56
6.2.2	Instantaneous adaptation	58
6.2.3	L_2 norm with P -regulator	58
6.2.4	L_2 norm with PD -regulator	61
6.2.5	H^{-1} norm with P -regulator	64
7	Conclusions & Summary	68
A	Inertial range in the Navier Stokes equation	70
B	Inertial range in the Kuramoto–Sivashinsky equation	72

Acknowledgements

I would like to thank my supervisor Dr. Bartosz Protas for introducing me to the problem described in this thesis and his willingness to share his knowledge and time with me. I would also like to thank my supervisory committee members Dr. Lightstone, Dr. Kevlahan and Dr. Nedialkov for taking time to review the thesis and giving helpful suggestions. I give my great appreciation to the faculty of the School Computational Engineering and Science for its support and insightful help.

Chapter 1

Introduction

1.1 Motivation

Many problems in science and engineering are not properly posed in the sense of Hadamard [1]. Here we present the definition of well posed problems.

Definition A solution to a mathematical problem is well posed in the sense of Hadamard if, in a given metric space,

- There exists a solution for all initial data.
- The solution is unique.
- The solution depends continuously on the initial data.

These problems come from a wide range of fields, for example reservoir engineering, seismology, meteorology, hydrodynamics and weather forecasting. But just because they are ill-posed does not diminish the importance of being able to solve these problems. Special care needs to be exercised to solve ill-posed problems. As regards evolutionary problems, the most classical case of a ill-posed problem is the terminal value problem of the heat equation. There have been a lot of research conducted at this particular problem. In this thesis we will look at the backward-in-time Kuramoto-Sivashinsky equation (KSE). The backward-in-time Kuramoto-Sivashinsky equation is nonlinear, which makes it more interesting than the terminal value problem for heat equation. The effect of the nonlinear term on the amount of regularization needed has not been studied in the past. There are

several established methods to use to solve approximately the terminal value problem for the heat equation; here we will apply two of them to the terminal value problem of the Kuramoto–Sivashinsky equation.

A motivation for pursuing this problem is the retrograde approach to variational data assimilation in numerical weather prediction. Data assimilation allows one to determine the initial condition for a weather forecast based on some observations of the atmosphere over some time period. The problem is that we would like to reconstruct the evolution of a system over $[0, T]$ based on incomplete and/or noisy measurements. One way of solving this problem is to optimize the initial data at $t = 0$, so the resulting system trajectory matches the available measurements as well as possible; thus this method requires repeated solution of the governing system over $[0, T]$ and the ad–joint system backwards over $[0, T]$. Note that both these systems are well–posed. The disadvantage of this approach is that using more measurements means moving the initial condition further into the past and therefore making it less relevant for a chaotic system such as the Earth’s atmosphere or the model problem we will be using, which is the Kuramoto–Sivashinsky equation.

This disadvantage disappears in the retrograde formulation [2], where we optimize for the terminal condition at $t = T$, instead of the initial condition. One problem is that the retrograde approach requires repeated solution of the governing system *backward* in time and the ad–joint system *forward* in time, both of which are ill–posed. Finding a good method solving these ill–posed problem would make this disadvantage of the retrograde approach disappear.

1.2 Regularization via solution of a less ill–posed problem

One way to solve ill–posed problems is to approximate their solutions by solutions of suitably–defined less ill–posed problems. Such problems can be obtained by adding a well–conceived term to the evolution equation in the original ill–posed problem. In the context of the backward heat equation such approach is known as “quasi–reversibility” [3]. The main problem is that we need to choose the magnitude of the regularization term so that the new

less ill-posed problem is stable and does not deviate too much from the original problem. While for linear problems such as the heat equation this issue is relatively well understood [3], little is known in the context of nonlinear problems. In addition to investigating this issue, in this thesis we also explore the possibility of an dynamic choice of the magnitude of the regularization term. We will attempt this by using simple concepts from control theory.

1.3 Structure of the thesis

Chapter 2 presents the Kuramoto–Sivashinsky equation. It introduces the two forms of the equation and shows how they are related. Also shown is the way of rescaling the Kuramoto–Sivashinsky equation to exhibit its dependence on a single parameter L . We also show the Fourier representation of the Kuramoto–Sivashinsky equation. This section also features a brief discussion about the energy function spectrum of a solution on the attractor for Kuramoto–Sivashinsky equation.

Chapter 3 is about the numerical schemes used to solve the Kuramoto–Sivashinsky equation. We will use the pseudo-spectral method together with a low-storage Runge–Kutta / Θ -method to solve this problem.

Chapter 4 addresses similarities and differences between the terminal value problem (TVP) for the heat equation and the terminal value problem for the Kuramoto–Sivashinsky equation. It features a proof (from [4]) that the terminal value problem for the heat equation is indeed ill-posed.

Chapter 5 deals with regularization techniques. It describes the regularization techniques that we choose to use and how we implemented them. The change of the energy function spectrum due to regularization is presented. The dynamic equations for the L_2 norm and the H^{-1} norms are derived and we show what effect regularization has on these norms. The last part of chapter 5 deals with different algorithms used to adapt the magnitudes of the regularization terms. Some of these algorithms are from classical control theory.

Chapter 6 features the computational results concerning the performance of the regularization–algorithms proposed in chapter 5.

Summary of the main results and final conclusions are deferred to chapter 7.

There are two appendices, Appendix A is a brief introduction to the “inertial range” phenomenology in the Navier Stokes equation. This is needed for Appendix B where the power law region of the energy function spectrum for the Kuramoto–Sivashinsky equation is examined.

Chapter 2

Kuramoto–Sivashinsky Equation (KSE)

The Kuramoto–Sivashinsky equation was proposed in [5] and [6] to model instabilities of a flame fronts. The Kuramoto–Sivashinsky equation is a good test case for nonlinear evolutionary system, because its solution features multiscale structures with characteristic length and time scales. It also has self sustained chaotic behaviour for large L . The Kuramoto–Sivashinsky equation was used to model flame fronts [6]. Our focus here will be entirely on the case with 1D periodic domain, $\Omega = [0, L]$. However all results can be generalized to a more complicated domains as in [2]. There are two different formulations of the Kuramoto–Sivashinsky equation:

- The *primitive* form

$$(2.1) \quad \left\{ \begin{array}{l} \frac{\partial v}{\partial \tau} + \frac{1}{2} \left(\frac{\partial v}{\partial x} \right)^2 + \frac{\partial^2 v}{\partial x^2} + \frac{\partial^4 v}{\partial x^4} = 0, \quad x \in \Omega, \quad \tau \in [0, T], \\ \frac{\partial^i v(0, \tau)}{\partial x^i} = \frac{\partial^i v(L, \tau)}{\partial x^i}, \quad \tau \in [0, T], \quad i = 0, \dots, 3, \\ v(x, 0) = \psi(x), \quad x \in \Omega. \end{array} \right.$$

The trouble with this form is that we have no bounds on the average of v in Ω [7]

$$(2.2) \quad \frac{\partial}{\partial t} \int_{\Omega} v(x, t) dx = -\frac{1}{2} \int_{\Omega} \left(\frac{\partial v(x, t)}{\partial x} \right)^2 dx = -\frac{1}{2} \int_{\Omega} (u(x, t))^2 dx.$$

To see this one needs to integrate (2.1) over domain Ω and the linear terms vanishes due to the boundary condition. Note that even if u is bounded as $t \rightarrow \infty$, there is no reason that the average of v to remain bounded.

- The *derivative* form of Kuramoto–Sivashinsky. This is obtained by setting $u = \partial v / \partial x$ in equation (2.1). Then we acquire the following equation,

$$(2.3) \quad \left\{ \begin{array}{l} \frac{\partial u}{\partial \tau} + u \frac{\partial u}{\partial x} + \frac{\partial^2 u}{\partial x^2} + \frac{\partial^4 u}{\partial x^4} = 0, \quad x \in \Omega, \quad \tau \in [0, T] \\ \frac{\partial^i u(0, \tau)}{\partial x^i} = \frac{\partial^i u(L, \tau)}{\partial x^i}, \quad \tau \in [0, T], \quad i = 0, \dots, 3, \\ u(x, 0) = \phi(x), \quad x \in \Omega. \end{array} \right.$$

This also means that

$$(2.4) \quad \int_0^L u(x) dx = 0.$$

In this research, the second form (2.3) of the Kuramoto–Sivashinsky equation is used. We need the solution of this initial value problem when T is large, the reason is that the solution should have reached its attractor. This attractor was shown by [8] to be connected and compact in the following space

$$(2.5) \quad \dot{L}^2(\Omega) = \left(u \in L^2(\Omega), \int_0^L u(x) dx = 0 \right).$$

So now we need to define the attractor set for the initial value problem of the Kuramoto–Sivashinsky equation [7].

Definition An attractor to Kuramoto–Sivashinsky is a set $\mathcal{A} \subset \dot{L}^2(\Omega)$ that has the following properties:

- \mathcal{A} is an invariant set.
- \mathcal{A} possesses an open neighbourhood \mathcal{U} such that, for every initial value $u_0 \in \mathcal{U}$, will converge to \mathcal{A} as $t \rightarrow \infty$.

When using the Kuramoto–Sivashinsky equation in hydrodynamic turbulence it is important that the solution has reached the attractor. If the solution is not at the attractor, we would observe transient behaviour instead of the statistical steady phenomena that we are interested in.

The terminal value problem which we want to solve is

$$(2.6) \quad \left\{ \begin{array}{l} \frac{\partial q}{\partial t} + q \frac{\partial q}{\partial x} + \frac{\partial^2 q}{\partial x^2} + \frac{\partial^4 q}{\partial x^4} = 0, \quad x \in \Omega, \quad t \in [0, T], \\ \frac{\partial^i q(0, t)}{\partial x^i} = \frac{\partial^i q(L, t)}{\partial x^i}, \quad t \in [0, T], \quad i = 0, \dots, 3, \\ q(x, T) = \varphi(x), \quad x \in \Omega. \end{array} \right.$$

The difference between (2.3) and (2.6) is that in the initial value problem we know the solution at $u(t = 0) \phi$ and in the terminal value problem we know the solution at $q(t = T) \varphi$. Solution of the initial value problem (2.3) exist for all square-integrable initial conditions $\phi(x)$. But for the terminal value problem (2.6) solution only exists when $\varphi(x)$ is on the attractor [9]. If $\varphi(x)$ is not on the attractor, we could even have a solution in which $\|u(\cdot, t)\|_{L_2}^2$ goes towards infinity faster than any exponential [10]. In other words, the solution to the terminal value problem will not exist in $[0, T]$, unless one makes sure that $\varphi(x)$ actually comes from a solution of an initial value problem (2.3) that has reached the attractor; only such terminal conditions will be considered in the present work.

2.1 Rescaling the Kuramoto–Sivashinsky equation

We want to show that the Kuramoto–Sivashinsky equation only depends on one parameter.

The most general form of this equation is

$$(2.7) \quad \left\{ \begin{array}{l} \frac{\partial q}{\partial t} + \alpha q \frac{\partial q}{\partial x} + \beta \frac{\partial^2 q}{\partial x^2} + \gamma \frac{\partial^4 q}{\partial x^4} = 0, \quad x \in [0, 2\pi], \quad t \in [0, T], \\ \frac{\partial^i q(0, t)}{\partial x^i} = \frac{\partial^i q(2\pi, t)}{\partial x^i}, \quad t \in [0, T], \quad i = 0, \dots, 3, \\ q(x, T) = \varphi, \quad x \in [0, 2\pi]. \end{array} \right.$$

So by rescaling we want to get

$$(2.8) \quad \left\{ \begin{array}{l} \frac{\partial \tilde{q}}{\partial \tilde{t}} + \tilde{q} \frac{\partial \tilde{q}}{\partial \tilde{x}} + \frac{\partial^2 \tilde{q}}{\partial \tilde{x}^2} + \frac{\partial^4 \tilde{q}}{\partial \tilde{x}^4} = 0, \quad \tilde{x} \in [0, L], \quad \tilde{t} \in [0, \tilde{T}], \\ \frac{\partial^i \tilde{q}(0, \tilde{t})}{\partial \tilde{x}^i} = \frac{\partial^i \tilde{q}(L, \tilde{t})}{\partial \tilde{x}^i}, \quad \tilde{t} \in [-\tilde{T}, 0], \quad i = 0, \dots, 3, \\ \tilde{q}(\tilde{x}, \tilde{T}) = \tilde{\varphi}, \quad \tilde{x} \in [0, L], \end{array} \right.$$

where L is now the only free parameter. This is the form often used in the literature. For large L the system becomes chaotic in space and time. The rescaling of equation (2.7) is

done by introducing the following variables

$$(2.9) \quad x = \zeta \tilde{x}, \quad t = \eta \tilde{t}, \quad q = \theta \tilde{q}.$$

This will change the equation into

$$(2.10) \quad \left\{ \begin{array}{l} \frac{\partial \tilde{q}}{\partial \tilde{t}} + \alpha \frac{\eta \theta}{\zeta} \tilde{q} \frac{\partial \tilde{q}}{\partial \tilde{x}} + \beta \frac{\eta}{\zeta^2} \frac{\partial^2 \tilde{q}}{\partial \tilde{x}^2} + \gamma \frac{\eta}{\zeta^4} \frac{\partial^4 \tilde{q}}{\partial \tilde{x}^4} = 0, \quad \tilde{x} \in [0, 2\pi/\zeta], \quad \tilde{t} \in [0, T/\eta], \\ \frac{\partial^i \tilde{q}(0, \tilde{t})}{\partial \tilde{x}^i} = \frac{\partial^i \tilde{q}(2\pi/\zeta, \tilde{t})}{\partial \tilde{x}^i}, \quad \tilde{t} \in [0, T/\eta], \quad i = 0, \dots, 3, \\ \tilde{q}(\tilde{x}, T) = \tilde{\varphi}, \quad \tilde{x} \in [0, 2\pi/\zeta]. \end{array} \right.$$

In order to determine the parameters characterizing this change of variables we need to solve the following system,

$$(2.11) \quad \alpha \frac{\eta \theta}{\zeta} = 1,$$

$$(2.12) \quad \beta \frac{\eta}{\zeta^2} = 1,$$

$$(2.13) \quad \gamma \frac{\eta}{\zeta^4} = 1.$$

By solving the above system we obtain the following relations,

$$(2.14) \quad \zeta = \sqrt{\frac{\gamma}{\beta}},$$

$$(2.15) \quad \eta = \frac{\gamma}{\beta^2},$$

$$(2.16) \quad \theta = \frac{1}{\alpha} \sqrt{\frac{\beta^3}{\gamma}}.$$

$$(2.17) \quad \left\{ \begin{array}{l} \frac{\partial \tilde{q}}{\partial \tilde{t}} + \tilde{q} \frac{\partial \tilde{q}}{\partial \tilde{x}} + \frac{\partial^2 \tilde{q}}{\partial \tilde{x}^2} + \frac{\partial^4 \tilde{q}}{\partial \tilde{x}^4} = 0, \quad \tilde{x} \in \left[0, 2\pi \sqrt{\frac{\beta}{\gamma}}\right], \quad \tilde{t} \in \left[0, T \frac{\beta^2}{\gamma}\right], \\ \frac{\partial^i \tilde{q}(0, \tilde{t})}{\partial \tilde{x}^i} = \frac{\partial^i \tilde{q}(2\pi \sqrt{\frac{\beta}{\gamma}}, \tilde{t})}{\partial \tilde{x}^i}, \quad \tilde{t} \in \left[0, T \frac{\beta^2}{\gamma}\right], \quad i = 0, \dots, 3, \\ \tilde{q}\left(\tilde{x}, T \frac{\beta^2}{\gamma}\right) = \tilde{\varphi}, \quad \tilde{x} \in \left[0, 2\pi \sqrt{\frac{\beta}{\gamma}}\right]. \end{array} \right.$$

Now we rescale it to L and \tilde{T} by the following relation

$$(2.18) \quad L = 2\pi \sqrt{\frac{\beta}{\gamma}}, \quad \tilde{T} = T \frac{\beta^2}{\gamma}.$$

which yields a equation system that depends only on one parameter

$$(2.19) \quad \left\{ \begin{array}{l} \frac{\partial \tilde{q}}{\partial t} + \tilde{q} \frac{\partial \tilde{q}}{\partial \tilde{x}} + \frac{\partial^2 \tilde{q}}{\partial \tilde{x}^2} + \frac{\partial^4 \tilde{q}}{\partial \tilde{x}^4} = 0, \quad \tilde{x} \in [0, L], \quad \tilde{t} \in [0, \tilde{T}], \\ \frac{\partial^i \tilde{q}(0, \tilde{t})}{\partial \tilde{x}^i} = \frac{\partial^i \tilde{q}(L, \tilde{t})}{\partial \tilde{x}^i}, \quad \tilde{t} \in [0, \tilde{T}], \quad i = 0, \dots, 3, \\ \tilde{q}(\tilde{x}, \tilde{T}) = \tilde{\varphi}, \quad \tilde{x} \in [0, L]. \end{array} \right.$$

2.2 Kuramoto–Sivashinsky equation in Fourier space

For the numerical solution of the Kuramoto–Sivashinsky equation we will employ the Fourier–Galerkin method [11]. The reason for using this method is its accuracy and computational efficiency. This is because of the periodic boundary condition and the way of calculating derivatives in Fourier space. We represent the solution in the following way

$$(2.20) \quad \hat{q}_\kappa(t) = \mathcal{F}(q) = \int_0^L q(x, t) e^{-i\kappa x} dx, \quad \kappa \in \mathbb{Z}.$$

Substituting (2.20) into (2.6) yields

$$(2.21) \quad \left\{ \begin{array}{l} \frac{\partial \hat{q}_\kappa}{\partial t} - \hat{w}_\kappa - \kappa^2 \hat{q}_\kappa + \kappa^4 \hat{q}_\kappa = 0, \quad \kappa \in \mathbb{Z}, \quad t \in [0, T], \\ \hat{q}_\kappa(T) = \hat{\varphi}_\kappa, \quad \kappa \in \mathbb{Z}, \end{array} \right.$$

where \hat{w}_κ is the nonlinear term in (2.6). Also note that since q is real, two Fourier modes corresponding to values of κ with opposite signs are complex conjugates, i.e. [11]

$$(2.22) \quad \hat{q}_{-\kappa} = \bar{\hat{q}}_\kappa,$$

where \bar{q} denotes the complex conjugate of q . To simplify the notation we will introduce

$$(2.23) \quad \left\{ \begin{array}{l} \frac{\partial \hat{q}_\kappa}{\partial t} = \hat{w}_\kappa + A \hat{q}_\kappa, \quad \kappa \in \mathbb{Z}, \quad t \in [0, T] \\ \hat{q}_\kappa(T) = \hat{\varphi}_\kappa, \quad \kappa \in \mathbb{Z}, \end{array} \right.$$

where $A \triangleq \kappa^2 - \kappa^4$ is the linear operator of the Kuramoto–Sivashinsky equation.

2.3 Form of the energy function spectrum

Since we are doing calculations in Fourier space it is useful to see which Fourier modes will inject energy and which will dissipate energy. These phenomenological observations

will shed some light on the physics represented by the Kuramoto–Sivashinsky equation and will also aid us in choosing physically motivated regularization strategies. The instantaneous amplitudes of the different Fourier modes can be seen in the energy function spectrum. Another thing we are interested in is the nonlinear transfer of energy between different Fourier modes. It is important to have a sense in which wavenumbers energy is created, destroyed, transported from and to. If this is understood it will be easier to find regularization strategies for the terminal value problem.

The energy function spectrum is defined by

$$(2.24) \quad E(\kappa) \triangleq \frac{1}{2} |\hat{u}_\kappa|^2, \quad \kappa \in \mathbb{Z}.$$

The typical appearance of the spectrum is a flat region for small wave numbers, a hump at the most energetic modes, a sub range with power law decay and exponential decay for the high wavenumbers. See figure 2.1 for a typical spectrum of a solution at the attractor.

The flat region corresponding to small wavenumber is similar to white noise [12]. A maximum approximately near $\kappa = 1/\sqrt{2}$, which can be used to get a typical length scale for the energetic modes. The region $0.8 \leq \kappa \leq 1.25$ has power law decay close to κ^{-4} [13], which is why it is sometimes referred to as an “inertial range” similar to the range found in Navier Stokes equation [14], for more information see Appendix A. For Fourier coefficients corresponding to high wave numbers the spectrum will go towards zero exponentially fast. The reason for that, is for a infinitely differentiable function which is periodic on $[0, L]$, Fourier coefficients will behave like [15]

$$(2.25) \quad \hat{u}_\kappa = O(e^{-\alpha\kappa}), \quad \text{for } \kappa \rightarrow \infty$$

where $\alpha > 0$.

Now we are going to focus on the power law region of the energy function spectrum. This power law region is supposed to be in between the large scales of the solution, where all the energy gets injected, and the small scales where the energy gets dissipated. All the energy flux towards higher wavenumber that goes through a wavenumber in the inertial

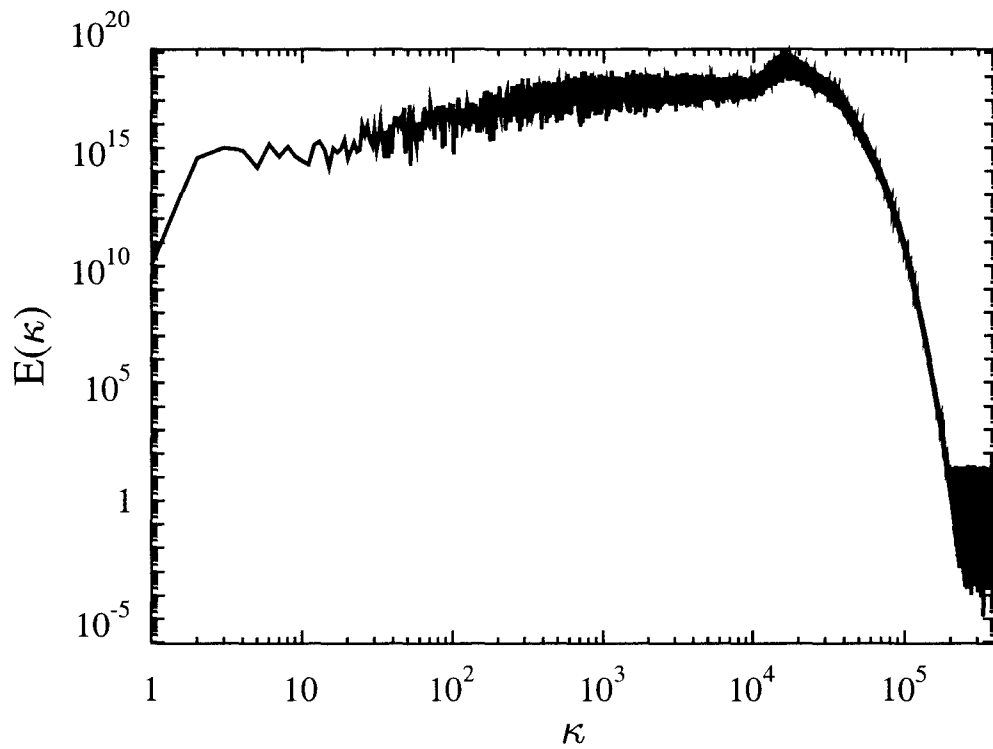


Figure 2.1: The energy function spectrum for a solution of the initial value problem (2.3).

range will get dissipated, where flux is defined as

$$(2.26) \quad F(\kappa) = \int_{\kappa}^{\infty} \hat{w}_{\bar{\kappa}} d\bar{\kappa} = \varepsilon,$$

where ε is the total dissipation for the system. And lastly the “inertial range” does not contain a lot of energy. For more details on how one makes the argument concerning existence of an “inertial range” in the Navier Stokes equation see Appendix A.

To ensure existence of an “inertial range” for the Kuramoto–Sivashinsky equation, the following assumptions have to be true [14];

- In the dissipating scales the energy flux due to nonlinear terms is equal to the dissipation

$$(2.27) \quad \frac{dF(\kappa)}{d\kappa} = -\kappa^4 E(\kappa).$$

- In the inertial sub range, no energy is lost or gained through the linearized part of the Kuramoto–Sivashinsky equation due to the shape of the energy function spectrum and

$$(2.28) \quad \frac{dF(\kappa)}{d\kappa} = 0.$$

- The flux past any wavenumber inside the inertial range is

$$(2.29) \quad F(\kappa) = \kappa^4 E(\kappa)$$

We do not believe that the power region which is seen in the energy function spectrum of the Kuramoto–Sivashinsky equation is an “inertial range”. We believe that the second assumption is only true at a point, but not in the whole power region. For more information we refer the reader to Appendix B.

Chapter 3

Numerical solution of the Kuramoto–Sivashinsky equation

We will use the truncated discrete Fourier representation of equation (2.23). This means that we will only use Fourier modes corresponding to wavenumbers ranging from zero to N . The terminal discrete value problem we are solving is thus

$$(3.1) \quad \begin{cases} \frac{\partial \hat{q}_\kappa}{\partial t} - \hat{w}_\kappa - A\hat{q}_\kappa = 0, & \kappa = 0, \dots, N, \quad t \in [0, T] \\ \hat{q}_\kappa(T) = \hat{\varphi}_\kappa, & \kappa = 0, \dots, N, \end{cases}$$

where the nonlinear term \hat{w}_κ is given by the convolution [11]

$$(3.2) \quad \hat{w}_k = i \sum_{\substack{l, m=0 \\ l+m=k}}^{N'} l \hat{q}_l \hat{q}_m, \quad \kappa = 0, \dots, N'.$$

where $N' > N$. We will see that the nonlinear term generates higher frequencies $N < \kappa < N'$, however they have to be truncated when we use a finite and fixed number of Fourier modes in equation (3.1). The symbol q represents the truncated solution to the terminal value problem. The discrete Fourier transform is defined as

$$(3.3) \quad \hat{q}_\kappa = \mathcal{F}(q) = \frac{1}{N} \sum_{i=1}^N q(x_i) e^{-i\kappa x_i}, \quad \kappa = 0, \dots, N.$$

where x_i are the discrete nodes in real space, defined as

$$(3.4) \quad x_i = \frac{iL}{N}, \quad i = 0, \dots, N.$$

To calculate this we will use the built-in command `fft` in MATLAB which is based on the library FFTW [16].

We want to calculate the nonlinear term in physical space not Fourier space, if we calculated it in Fourier space, we would need to evaluate the convolution sum (3.3) which requires $O(N^2)$ arithmetic operations. On the other hand, because of the efficiency of FFT, evaluating the nonlinear term in physical space requires only $O(N \log(N))$ arithmetic operations. Thus calculate the nonlinear term using the following expression [11]

$$(3.5) \quad \hat{w}'_{\kappa} = \frac{1}{N} \sum_{i=1}^N w(x_i) e^{-i\kappa x_i}, \quad \kappa = 0, \dots, N$$

where

$$(3.6) \quad w(x_i) = q(x_i) \frac{\partial q(x_i)}{\partial x}, \quad i = 0, \dots, N.$$

Since \hat{w}_{κ} is the expression we want to calculate in our PDE problem (3.1). We want to examine the difference between \hat{w}'_{κ} and \hat{w}_{κ} . This difference has to do with the so-called “aliasing errors” related to the fact that when the nonlinear term is evaluated in real space (3.6), the higher modes generated by this term (i.e. with $N < \kappa < N'$) are not truncated, but instead become “aliased” to lower wavenumber modes [17]. If we insert equation (3.6) into equation (3.5) we get that

$$(3.7) \quad \begin{aligned} \hat{w}'_{\kappa} &= \frac{1}{N} \sum_{i=1}^N \left(\sum_l q_l e^{ilx_i} \right) \left(\sum_m imq_m e^{imx_i} \right) e^{-i\kappa x_i} = \\ &= \frac{1}{N} \sum_{i=1}^N \sum_{l,m} lq_l q_m e^{i(l+m-\kappa)x_i}, \quad \kappa = 0, \dots, N, \end{aligned}$$

then using [11]

$$(3.8) \quad \sum_{i=1}^N e^{i(k-l)\frac{2\pi i}{N}} = \begin{cases} N & \text{if } k-l = mN, \quad m = 0, \pm 1, \pm 2, \dots, \\ 0 & \text{otherwise,} \end{cases}$$

we will end up with the following link between the aliased \hat{w}' and original terms \hat{w} (\hat{w} is defined in 3.2)

$$(3.9) \quad \hat{w}'_{\kappa} = \hat{w}_{\kappa} + i \sum_{\substack{l,m \\ l+m=k+N}} l\hat{q}_l \hat{q}_m + i \sum_{\substack{l,m \\ l+m=k-N}} l\hat{q}_l \hat{q}_m, \quad \kappa = 0, \dots, N.$$

If we ignore this difference between the expressions \hat{w}_κ and \hat{w}'_κ , then the higher-wavenumber Fourier modes that should not be resolved will be “aliased” on the Fourier modes that are resolved. To prevent this we will use the “3/2 rule” [18]. We are going to add Fourier modes corresponding to higher wavenumbers and set their amplitudes equal to zero. This means that we also change the grid size in physical space from N to $N' = 3N/2 + 1$. This will in turn change equation (3.9) into

$$(3.10) \quad \tilde{w}_\kappa = \hat{w}_\kappa + i \sum_{\substack{l,m \\ l+m=k+N'}} l \hat{q}_l \hat{q}_m + i \sum_{\substack{l,m \\ l+m=k-N'}} l \hat{q}_l \hat{q}_m, \quad \kappa = 0, \dots, N'.$$

And since the newly added Fourier modes are equal to zero, the sums on the right hand side are cancelled and we thus obtain

$$(3.11) \quad \tilde{w}_\kappa = \hat{w}_\kappa.$$

We remark that since FFTs are performed on the extended grids with N' points, we set N' equal to an integer power of 2 which ensures the best performance of FFT. This sequence of steps is summarized in algorithm 1. This is called de-aliasing.

Input: The Fourier coefficients \hat{u}

Output: The nonlinear term \tilde{w}

Calculate u by IFFT;

$u = \text{IFFT}(\hat{u});$

Multiply u with itself and divide by two;

Then take the Fourier transform of the result;

$\bar{w} = \text{FFT}(u^2/2);$

Multiply with κ to get $\tilde{w}_\kappa;$

$\tilde{w} = \kappa \cdot \bar{w};$

Algorithm 1: Calculation of the nonlinear term

Since we are evaluating the nonlinear terms in real space and all the space derivatives in Fourier space, the resulting method is called pseudo-spectral.

There are several choices regarding discretization in time of a system of nonlinear ordinary differential equations (ODE) as in (3.1). Below we present a general approach considered most appropriate for evolutionary systems of type (3.1):

- explicit treatment of the nonlinear term which effectively linearize this term, therefore avoiding the solution of a dense nonlinear algebraic system at every time step. This means that to nonlinear term will be calculated with information from previous sub steps.
- implicit treatment of the linear terms which bypasses the stability limitations due to high-order derivatives; since differential operators are diagonal in Fourier representation, no algebraic system needs to be solved as a result of this implicit treatment.

To accomplish this we will use the low-storage Runge-Kutta method (RKW3) described by [19] combined with the Θ -method. This method uses three sub steps for each time step. One needs to define the following coefficients

$$(3.12) \quad \Theta = 0.75, \quad \bar{\beta} = \begin{pmatrix} 4/15 \\ 1/15 \\ 1/6 \end{pmatrix}, \quad \bar{\gamma} = \begin{pmatrix} 8/15 \\ 5/12 \\ 3/4 \end{pmatrix}, \quad \bar{\zeta} = \begin{pmatrix} 0 \\ -17/60 \\ -5/12 \end{pmatrix},$$

o that for each sub step we need to solve the following equation,

$$(3.13) \quad \left(I + \frac{\Theta}{2} \Delta t \bar{\beta}_{rk} A \right) \hat{y}_{\kappa}^{rk+1} = \hat{y}_{\kappa}^{rk} - \Delta t \left(\frac{1 - \Theta}{2} \bar{\beta}_{rk} A \hat{y}_{\kappa}^{rk} + \bar{\gamma}_{rk} r(\hat{y}_{\kappa}^{rk}) + \bar{\zeta}_{rk} r(\hat{y}_{\kappa}^{rk-1}) \right), \quad rk = 1, 2, 3, \quad \kappa = 1, \dots, N,$$

where A is the linear operator described in equation (2.23) and $r(\hat{y}_{\kappa}^{rk})$ is the nonlinear term denoted above with the symbol \hat{w}_{κ} . Note also that $y^0 = \hat{u}(t^n)$ and $y^4 = \hat{u}(t^{n+1})$. So $\bar{\beta}_{rk}$, $\bar{\gamma}_{rk}$ and $\bar{\zeta}_{rk}$ describe the different weights assigned to the linear and nonlinear terms at different sub steps. Because $\Theta = 0.75$ the calculation will be skewed towards the implicit method.

Chapter 4

Analogies between the TVP for the heat equation and the KSE

The Kuramoto–Sivashinsky equation has certain similarities to the heat equation. Since the terminal value problem of the heat equation is well-understood, we consider it briefly here in order to understand the origins of ill-posedness in backward evolutionary problems such as the Kuramoto–Sivashinsky equation. We will also comment on the difference between the two problems. The backwards heat equation is

$$(4.1) \quad \begin{cases} \frac{\partial v}{\partial \tau} + c \frac{\partial^2 v}{\partial x^2} = 0, & x \in \Omega, \quad \tau \in [0, T], \\ v(0, \tau) = v(2\pi, \tau), & \tau \in [0, T], \\ v(x, 0) = \Phi, & x \in \Omega. \end{cases}$$

Now look at the Fourier formulation of the problem

$$(4.2) \quad \begin{cases} \frac{\partial \hat{v}_\kappa}{\partial \tau} - c\kappa^2 \hat{v}_\kappa = 0, & \kappa \in \mathbb{Z} \quad \tau \in [0, T], \\ \hat{v}_\kappa(0) = \hat{\Phi}_\kappa, & \kappa \in \mathbb{Z}, \end{cases}$$

where if c is positive this is an ill-posed problem. The proof that the inverse heat problem is ill-posed in the sense of Hadamard is from [4].

Theorem 1 *Consider solution of (4.1) evaluated at $t = T$ $f = v(x, T)$, where $\Phi, f \in L_2$, then f does not depend continuously on Φ , that is, the problem (4.1) is ill-posed in the sense of Hadamard, since the stability requirement is not satisfied.*

Proof Start by assuming that you have two different initial conditions, $\Phi_1, \Phi_2 \in L_2(\Omega_2)$.

To make it easier $\Omega_2 \in [0, 1]$. Let the two initial conditions are related by the following

condition

$$(4.3) \quad \Phi_2 = \Phi_1 + Ke^{-c(m\pi)^2T} \cos(m\pi),$$

with $K \in \mathbb{R}$, and m is an integer. Now look at the difference between two solutions f_1, f_2 at time $t = 0$ for the two different initial conditions. This means that one can express f_2 as a function of f_1 by using linearity

$$(4.4) \quad f_2(x) = f_1(x) + K \cos(m\pi).$$

So the difference between them is given by

$$(4.5) \quad \|\Phi_2 - \Phi_1\|_2^2 = \int_{\Omega_2} |\Phi_2(x, \tau) - \Phi_1(x, \tau)|^2 dx = K^2 e^{-2c(m\pi)^2T} \int_{\Omega_2} \cos^2(m\pi x) dx.$$

If one measures the difference between Φ_1 and Φ_2 , one would obtain

$$(4.6) \quad \|f_1 - f_2\|_2^2 = K^2 \int_{\Omega_2} \cos^2(m\pi x) dx = \frac{K^2}{2}.$$

for all m . Making m large, one gets the following limits

$$(4.7) \quad \|\Phi_2 - \Phi_1\|_2 \rightarrow 0, \quad \|f_2 - f_1\| \not\rightarrow 0.$$

So the inverse heat problem is ill-posed in the sense of Hadamard. ■

Note also that

$$(4.8) \quad \|\Phi_2 - \Phi_1\|_2 = e^{-c(m\pi)^2\tau} \|f_2 - f_1\|_2.$$

This makes it clear that any noise from $t = 0$ will grow exponentially in the problem. The problem we are to look into is slightly different. The Kuramoto–Sivashinsky terminal value problem has a nonlinear term and the inverse heat equation does not. This means that the inverse heat equation lacks spectral transfer between different Fourier modes. This makes it impossible for the modes corresponding to the large wavenumbers to lose energy. This means that any small perturbation in a Fourier node corresponding to large wavenumber will grow as time goes by.

For the Kuramoto–Sivashinsky equation we have a non linear term that transfers energy between different Fourier modes. This transfer in the initial value problem move in average

energy from the Fourier modes corresponding to small wavenumbers into the Fourier modes corresponding to large wavenumber. The spectral transfer may help stabilize the solution to the terminal value problem, if it transfers energy from the Fourier modes corresponding to large wavenumber into Fourier modes corresponding to small wavenumber. So the term that was the source of a number of complications in the initial value problem might help us in the terminal value problem. For results on the regularization of the linearized Kuramoto–Sivashinsky equation see section 6.1.1.

Chapter 5

Regularization of the terminal value problem

5.1 General remarks

To solve the terminal value problem (3.1), we first have to solve the initial value problem

$$(5.1) \quad \begin{cases} \frac{\partial \hat{u}_\kappa}{\partial t} - \hat{w}_\kappa - \kappa^2 \hat{u}_\kappa + \kappa^4 \hat{u}_\kappa = 0, & \kappa = 0, \dots, N \quad \tau \in [0, T], \\ \hat{u}_\kappa(0) = \hat{\phi}_\kappa, & \kappa = 0, \dots, N \end{cases}$$

Then we will use the solution obtained at the last time step as a starting point for the solution of the terminal value problem. It is important that the terminal value for the backward problem be on the attractor \mathcal{A} . Otherwise one can not be sure that the terminal value problem has a solution. How do we know if this is true? For sufficiently large L the energy of the solution trajectory at the attractor \mathcal{A} oscillates around a fixed value, it is not constant, but varies within a few percent of the mean value (see figure 5.1). We must also check that the energy function spectrum looks as described in section 2.3, note that the Fourier modes corresponding to the small wavenumber will require the most time to reach the desired value. The difference between the terminal value problem and the initial value problem is where we know the solution. In the initial value problem, we know the solution at $t = 0$ and in the terminal value problem we know the solution at $t = T$. We can turn the terminal value problem into a initial value problem by making the following change of variables

$$(5.2) \quad \tau \triangleq T - t.$$

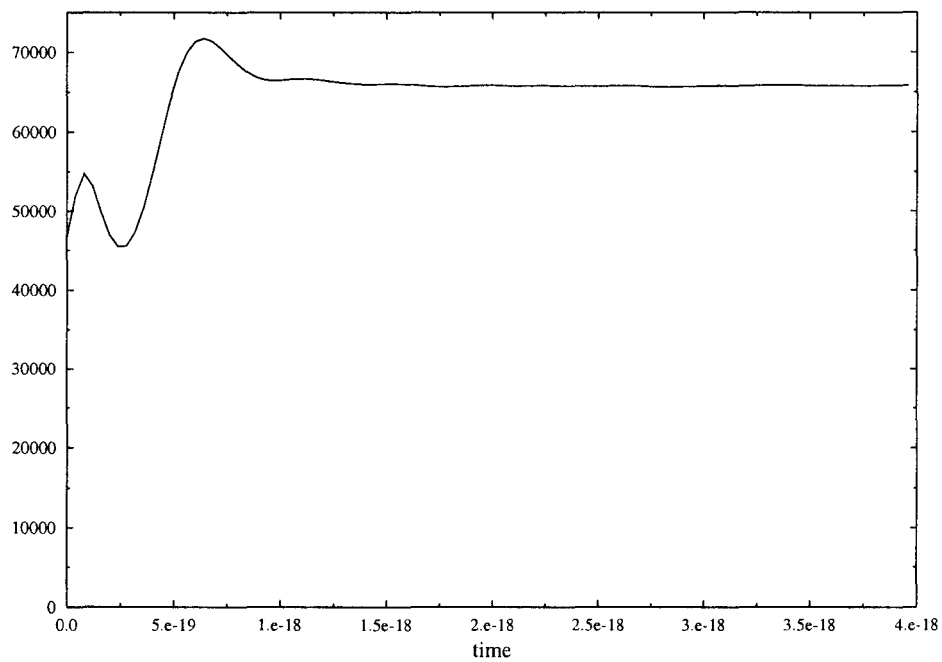


Figure 5.1: Energy for the solution to the initial value problem when initial value is a sine wave with period L .

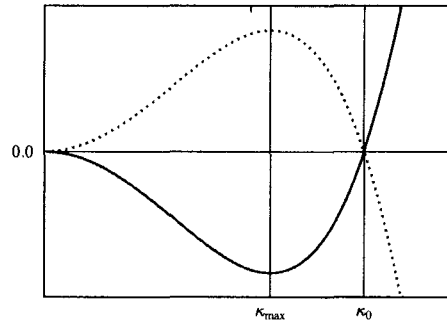


Figure 5.2: Linearized operator for Kuramoto–Sivashinsky for different directions of time, (dotted line) for the forward problem ($0 \rightarrow T$), (solid line) for the backward problem ($0 \leftarrow T$).

This will change (3.1) into the following problem

$$(5.3) \quad \begin{cases} \frac{\partial \hat{q}_\kappa}{\partial \tau} + \hat{w}_\kappa + A \hat{q}_\kappa = 0, & \kappa = 0, \dots, N, \quad \tau \in [0, T] \\ \hat{q}_\kappa(0) = \hat{\varphi}_\kappa, & \kappa = 0, \dots, N. \end{cases}$$

By comparing this equation and (5.1) we can see that role of the terms κ^2 and κ^4 are reversed. In the initial value problem the term κ^2 injects energy and the term κ^4 dissipates energy. In the terminal value problem the κ^2 term dissipates energy and the κ^4 term injects energy. This is easily seen if one looks at the linearized operator A defined in equation (2.23) and compare it the linearized operator B defined as

$$(5.4) \quad B = -A = -\kappa^2 + \kappa^4.$$

Reformulation of the problem will make the Kuramoto–Sivashinsky lose some of its properties when time is reversed, see figure 5.2. Large time stability that was proved by [8] for the initial value problem is not valid for the terminal value problem. This equation without regularization will diverge super-exponentially fast when solved numerically. This effect is illustrated in 5.3.

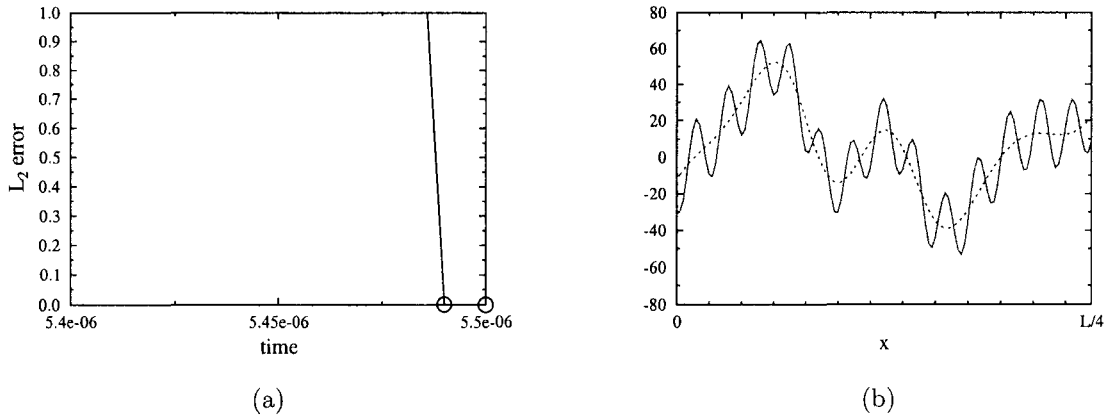


Figure 5.3: (a) L_2 error for the solution to the terminal value problem without any regularization. Note that only the first couple of points are finite. (b) Comparison between the solution to the initial value problem (dashed line) and the solution to the terminal value problem (solid line) without regularization at $t = 5.49 \cdot 10^{-6}$. The solution to the terminal value problem has more small scale features.

5.2 Regularization techniques

Since this terminal value problem is strongly ill-posed we need to regularize it. In the spirit of the quasi-reversibility method developed by [3], we propose to transform the original ill-posed problem (3.1) into a well-posed, or a less ill-posed, problem. We will do this by adding a regularizing term $\hat{\mathcal{B}}\hat{u}_\kappa$, which yields

$$(5.5) \quad \begin{cases} \frac{\partial \hat{p}_\kappa}{\partial t} - \hat{w}_\kappa + B\hat{p}_\kappa - \nu \hat{\mathcal{B}}\hat{p}_\kappa = 0, & \kappa = 0, \dots, N, \quad t \in [0, T], \\ \hat{p}_\kappa(T) = \hat{\varphi}_\kappa, & \kappa = 0, \dots, N \end{cases}$$

where $\nu \in \mathbb{R}_+$ and \mathcal{B} is some operator acting on \hat{u} . See [3] for different operators that can be used to regularize this terminal value problem. Here we will concentrate on two methods described in that research, we will call them hyperviscous and pseudo-parabolic regularization. We want ν to be as small as possible so the regularized equation is close to (3.1). On the other hand if ν is too small, then the regularized equation will have the same problem as (3.1). Namely, amplitudes of some Fourier modes will tend towards infinity. Continuous dependence on the regularization coefficients was proved for the two methods listed below in [20] in the case of the backward heat equation. Here we assume

that there is continuous dependence on the regularization coefficients for the backwards Kuramoto–Sivashinsky equation.

5.2.1 Hyperviscous regularization

This technique was suggested in [3]. We will modify the terminal value problem of the Kuramoto–Sivashinsky equation by adding a higher-order term. This will prevent the coefficients with high wavenumbers from getting too much energy and make the L_2 norm of the solution of the terminal value problem go towards infinity. We choose to add a sixth order term so that the governing equation will thus become

$$(5.6) \quad \frac{\partial u}{\partial t} + u \frac{\partial u}{\partial x} + \frac{\partial^2 u}{\partial x^2} + \frac{\partial^4 u}{\partial x^4} + \nu_6 \frac{\partial^6 u}{\partial x^6} = 0, \quad x \in \Omega$$

This equation is well-posed. This extra term will prevent too much energy from getting injected at the highest wave number, but this extra term will also make the solution to the perturbed equation to have less energy than the solution to the original terminal value problem. Choosing ν_6 too small will not be sufficient to stabilize the problem, whereas and choosing it too large makes the backwards solution to decay too rapidly. This is more easily seen if we were to look at the regularized Kuramoto–Sivashinsky equation in Fourier space

$$(5.7) \quad \frac{\partial \hat{p}_\kappa}{\partial t} + \hat{w}_\kappa + B \hat{p}_\kappa - \nu_6 \kappa^6 \hat{p}_\kappa = 0, \quad \kappa = 0, \dots, N.$$

5.2.2 Pseudo-parabolic regularization

Another option is to add a term which has both time and space derivatives. According to [20] such equations have been called pseudo-parabolic by [21] and been used in the context of backward-in-time problem by [22], [23] and [24]. So the backwards regularized problem will now take the following form

$$(5.8) \quad \frac{\partial u}{\partial t} + u \frac{\partial u}{\partial x} + \frac{\partial^2 u}{\partial x^2} + \frac{\partial^4 u}{\partial x^4} + \nu_{dt} \frac{\partial}{\partial t} \frac{\partial^4 u}{\partial x^4} = 0, \quad x \in \Omega.$$

Note that this problem is not well-posed, however it is less ill-posed than the original problem. If we allow the value of ν_{dt} to be negative we get a pole at $\kappa_p = (-1/\nu_{dt})^{1/4}$.

This can be seen in the Fourier form of the regularized equation (5.8),

$$(5.9) \quad \frac{\partial \hat{p}_\kappa}{\partial t} = \frac{-\hat{w}_\kappa + \kappa^2 \hat{p}_\kappa - \kappa^4 \hat{p}_\kappa}{1 + \nu_{dt} \kappa^4 \hat{p}_\kappa}, \quad \kappa = 0, \dots, N$$

We will allow negative values as long as $\kappa_p > N$. However negative values will amplify the energy injection at Fourier modes corresponding to high wavenumbers. Which will make the problem harder to solve, because the reason that the back-ward-in-time problem is hard to solve is the energy injected at small scales.

5.3 Spectrum change due to regularization

The regularization technique will change the energy spectrum because we are not solving the same equation backwards as we solved in the forward problem. The change can be noticeable as seen in figure 5.4. Here the spectrum has a lot more energy in the smaller scale when t is close to T than when $t = 0$. To understand why we need to look at the effect ν_6 and ν_{dt} has not just on the high κ , but also the effect on Fourier modes with low wavenumbers. To see this more clearly we look at the Kuramoto–Sivashinsky equation with the nonlinear term removed and we will also look at the problem for a initial value viewpoint so time will move in the positive direction,

$$(5.10) \quad \frac{d\hat{p}_\kappa}{d\tau} = B\hat{p}_\kappa, \quad \kappa \in \mathbb{Z}$$

Notice that for the pseudo-parabolic regularization the spectrum looks much better than in the hyperviscous case, see figure 5.5.

5.3.1 The low wavenumber part of the spectrum

The linearized operator B will have one extreme point at $\kappa = 1/\sqrt{2}$. If we do the same when we add a hyperviscous perturbation we end up with

$$(5.11) \quad g(\kappa) = (B - \nu_6 \kappa^6) = -\kappa^2 + \kappa^4 - \nu_6 \kappa^6.$$

This function has the one extreme point at

$$(5.12) \quad \kappa_{max} = \frac{\sqrt{1 - \sqrt{1 - 3\nu_6}}}{\sqrt{3\nu_6}}$$

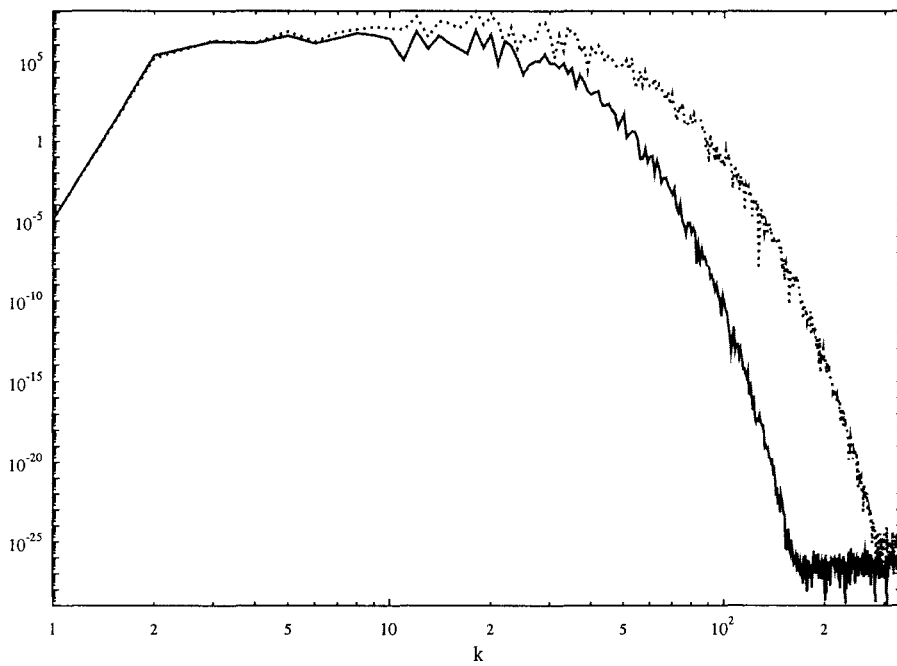


Figure 5.4: Energy spectrum of a solution with a fixed value of ν_6 at $t = 0$, solid line, and $t = T$, dotted line, of the terminal value problem.

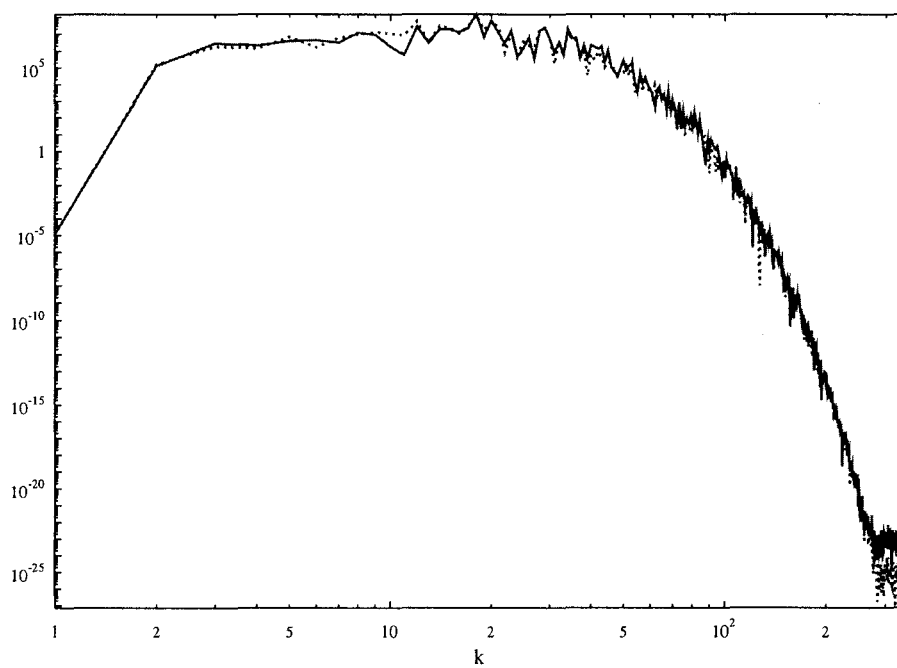


Figure 5.5: Energy spectrum of a solution with a fixed value of ν_{dt} at $t = 0$, solid line, and $t = T$, dotted line, of the terminal value problem.

We are interested in this point, because in the forward run this point is closely related with where most the energy is injected. The other points are uninteresting. Two are negative and one is at higher wavenumbers. Also notice that this function will have the peak switched to the higher wavenumbers. This means that when we are doing the backwards run we should see a change of where the most energetic modes are. They should be displaced into higher wavenumbers.

If we try to do the same thing for the technique the mixed time and space derivatives we get that

$$(5.13) \quad h(\kappa) = \frac{B}{1 + \nu_{dt}\kappa^4} = \frac{-\kappa^2 + \kappa^4}{1 + \nu_{dt}\kappa^4}.$$

The extreme point we are interested in is

$$(5.14) \quad \kappa_{max} = \frac{\sqrt{\sqrt{1 + \nu_{dt}} - 1}}{\sqrt{\nu_{dt}}}$$

The high wavenumbers are dampened as the previous regularization techniques. The peak of the linearization is switched to higher wavenumbers just as in the case of the hyperviscous technique. This can be seen in figure 5.6.

5.3.2 The high wavenumber part of spectrum

In this section we will look at the Fourier modes where energy will be injected when we solve the terminal value problem. The idea is to dampened the amount of energy injected into the Fourier modes that correspond to high wavenumbers to make sure that these Fourier modes do not grow too large. We want to look at two things, one is at which wavenumber there is now injection or dissipation of energy, the other is how much damping is made on the high Fourier modes. The first one will show where the power law region might be for the solution to the terminal value problem.

If one adds hyperviscous dissipation to the Kuramoto–Sivashinsky equation, one point inside the power law region will change from $\kappa_0 = 1$ to the following wavenumber

$$(5.15) \quad \kappa_0 = \sqrt{\frac{1 - \sqrt{1 - 4\nu_6}}{2\nu_6}}.$$

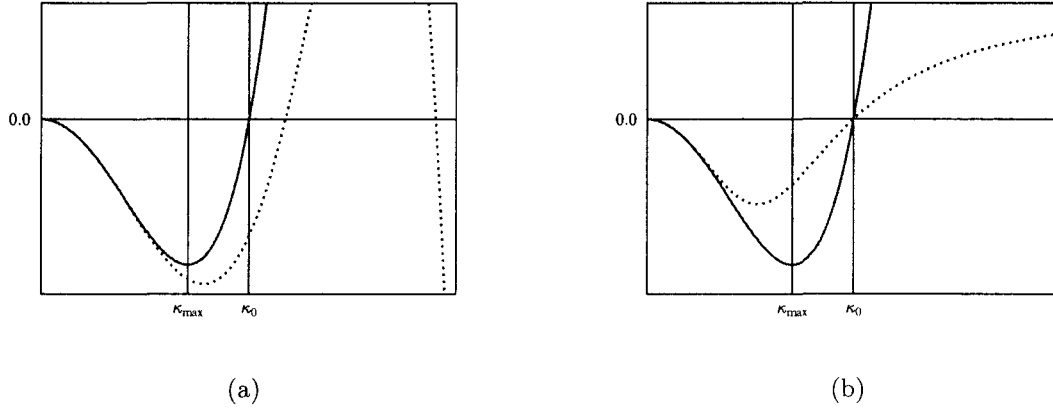


Figure 5.6: A qualitatively sketch of the effect of regularization. (a) hyperviscous regularization and (b) Pseudo–parabolic regularization. Linearized operator (solid line) and regularized operator (dotted line). The symbols κ_{max} and κ_0 are the values of the wavenumber where the operator A , respectively, has a maximum value and is equal to zero (see section 5.3.1).

This method of regularization will move the power law region to a higher wavenumber. One can see the effect in figure 5.6. Note that this is the linearized form of Kuramoto–Sivashinsky, however the power law region should contain the point κ_0 in the original equation as well.

The pseudo–parabolic method will not change the position of this wavenumber (κ_0).

So these regularization techniques will dampen the Fourier modes corresponding to higher wavenumbers more efficiently than the non–regularized equation. This is very important because otherwise small perturbations in high Fourier modes will grow very quickly and make the solution diverge.

Now we need to remember that we did the following change of variables $\tau = T - t$, this means that we moved the terminal value problem into a initial value problem. So this means that for the solution to the regularized problem all these shifts will be in the other way. So a shift to higher wavenumber will result in the regularized solution at $t = 0$ to shift into lower wavenumber.

5.4 Energy, L_2 norm

Here we derive the conditions for the L_2 norm to be constant with respect to time. This condition will then be used in section 5.6 to adjust adaptively the values of the regularization parameters. So far we have assumed that the energy is constant, but what do we require for this to be true? Start by looking at the energy equation for the Kuramoto–Sivashinsky equation in Fourier space

$$(5.16) \quad \frac{dE}{dt} = \frac{d}{dt} \frac{1}{2} \sum_{\kappa=1}^{\infty} |\hat{u}_{\kappa}|^2 = \frac{1}{2} \sum_{\kappa=1}^{\infty} \kappa^2 |\hat{u}_{\kappa}|^2 - \kappa^4 |\hat{u}_{\kappa}|^2$$

Notice that the nonlinear term has disappeared, which is because when one averages over all Fourier modes the sum is zero. This is true in a domain with periodic boundary conditions. The proof of this is the same as for Navier Stokes

$$(5.17) \quad \int_0^L u \frac{\partial u}{\partial x} u dx = \frac{1}{3} \int_0^L \frac{\partial uuu}{\partial x} dx = [uuu]_0^L = 0$$

By Parseval's theorem, (5.16) is the same as multiplying (2.21) with u and take the integral over Ω . Since the boundary conditions are periodic, the value of u at $x = 0$ and at $x = L$ are the same. To calculate the L_2 norm

$$(5.18) \quad E(t) = \frac{1}{2} \sum_{\kappa=1}^N |\hat{u}_{\kappa}|^2.$$

And the dynamic equation (5.16) will change into

$$(5.19) \quad \frac{dE}{dt} = \frac{d}{dt} \frac{1}{2} \sum_{\kappa=0}^N |\hat{u}_{\kappa}|^2 = \sum_{\kappa=1}^N \kappa^2 |\hat{u}_{\kappa}|^2 - \sum_{\kappa=1}^N \kappa^4 |\hat{u}_{\kappa}|^2.$$

Now we will see how the different methods of regularization will change the energy equation.

5.4.1 Energy equation for hyperviscous regularization technique

By including the higher order term we are adding hyperviscous dissipation to the flow, which means that in this approach will try and remove energy from the flow by means of a $\int_{-\infty}^{\infty} \kappa^6 |\hat{u}_{\kappa}|^2 d\kappa$ term. So the energy equation will change into

$$(5.20) \quad \frac{dE}{dt} = \sum_{\kappa=1}^{\infty} \kappa^2 |\hat{p}_{\kappa}|^2 - \kappa^4 |\hat{p}_{\kappa}|^2 + \nu_6 \kappa^6 |\hat{p}_{\kappa}|^2.$$

Note that we will solve the equation backwards-in-time. So the larger the value of ν_6 one uses, the more energy is removed from the system. If the energy is high, increase ν_6 . If it is too low, decrease ν_6 .

5.4.2 Energy equation for the pseudo-parabolic technique

By adding the mixed space and time derivative the results are not as straight forward. In this case the energy equation changes into

$$(5.21) \quad \frac{dE}{dt} = \sum_{\kappa=1}^{\infty} \kappa^2 |\hat{p}_\kappa|^2 - \kappa^4 |\hat{p}_\kappa|^2 + \nu_{dt} \frac{d}{dt} \kappa^4 |\hat{p}_\kappa|^2.$$

So whether or not the last term will increase or decrease the energy during the backwards run depends on the sign of ν_{dt} and $\frac{d}{dt} \sum_{\kappa=1}^{\infty} \kappa^4 |\hat{p}_\kappa|^2$. So if the energy of the high wavenumbers increase during the backwards run and ν_{dt} is positive this will remove energy from the domain. The effect on the spectrum will be bigger on the Fourier modes corresponding to large wavenumbers than the Fourier modes corresponding to small wavenumber. This is easily seen if one looks at the linearized forms of the operator. We will use a positive value of ν_{dt} because of its behaviour in the linearized operator. The other reason is that if the norm $\sum_{\kappa=1}^{\infty} \kappa^4 |\hat{u}_\kappa|^2$ grows we need to decrease the energy in the backwards run. If $\nu_{dt} \rightarrow \infty$, then

$$(5.22) \quad \frac{d}{dt} \sum_{\kappa=1}^{\infty} \kappa^4 |\hat{p}_\kappa|^2 = 0.$$

So for large value of ν_{dt} we will have the effect of freezing this norm.

5.5 H^{-1} norm

Instead of choosing the L_2 norm to be constant, we can use a different norm. For example we can look at H^{-1} , this norm concentrates on the large scales of the problem. This norm can be obtained by

$$(5.23) \quad \|\hat{q}\|_{H^{-1}} = \frac{1}{2} \sum_{\kappa=1}^N \frac{|\hat{q}_\kappa|^2}{\kappa^2}.$$

Note that this is similar to taking the L_2 norm of the primitive form of the Kuramoto–Sivashinsky equation (2.1). To see how we can change the coefficient of the regularization we need to look at the dynamic equation for the H^{-1} norm. To get the norm we multiply the dynamic equation with a function φ which has the following properties

$$(5.24) \quad \begin{cases} \Delta\varphi = q, & x \in [0, L] \\ \frac{\partial^i \varphi(0)}{\partial x^i} = \frac{\partial^i \varphi(L)}{\partial x^i}, & i = 0, \dots, 2. \end{cases}$$

Integrate from zero to L to get

$$(5.25) \quad \int_0^L \frac{\partial q}{\partial t} \varphi dx + \int_0^L q \frac{\partial \varphi}{\partial x} dx + \int_0^L \frac{\partial^2 q}{\partial x^2} \varphi dx + \int_0^L \frac{\partial^4 q}{\partial x^4} \varphi dx = 0.$$

Then use Parseval's theorem to go into Fourier space

$$(5.26) \quad \sum_{\kappa=1}^{\infty} \frac{\partial \hat{q}}{\partial t} \hat{\varphi} + (\hat{q} * i\kappa \hat{q}) \hat{\varphi} + (i\kappa)^2 \hat{q} \hat{\varphi} + (i\kappa)^4 \hat{q} \hat{\varphi} = 0.$$

Where $\hat{q} * \hat{v}(\kappa)$ is the convolution defined by

$$(5.27) \quad \hat{q} * \hat{v}(\kappa) = \sum_{\substack{l,m=0 \\ l+m=\kappa}}^{N'} \hat{q}_l \hat{v}_m, \quad \kappa = 0, \dots, N'.$$

And since $(i\kappa)^2 \hat{\varphi} = \hat{q}$ we end up with

$$(5.28) \quad - \sum_{\kappa=0}^{\infty} \frac{\partial \hat{q}}{\partial t} \frac{\hat{q}}{\kappa^2} - (\hat{q} * i\kappa \hat{q}) \frac{\hat{q}}{\kappa^2} + |\hat{q}|^2 - \kappa^2 |\hat{q}|^2 = 0.$$

Rewrite it in a simpler form

$$(5.29) \quad \frac{1}{2} \frac{d}{dt} \sum_{\kappa=1}^{\infty} \frac{|\hat{q}|^2}{\kappa^2} = -i \sum_{\kappa=0}^{\infty} \frac{(\hat{q} * \kappa \hat{q}) \hat{q}}{\kappa^2} + |\hat{q}|^2 - \kappa^2 |\hat{q}|^2.$$

To see if the nonlinear term is zero in this norm as it was in the L_2 norm, start by looking at the nonlinear term in physical space,

$$(5.30) \quad \int_0^L q \frac{\partial q}{\partial x} \varphi dx = \frac{1}{2} \int_0^L \frac{\partial qq}{\partial x} \varphi dx = \frac{1}{2} \left([qq\varphi]_0^L - \int_0^L qq \frac{\partial \varphi}{\partial x} dx \right) = \\ = -\frac{1}{2} \left(\int_0^L qq \frac{\partial \varphi}{\partial x} dx \right) = \hat{W}.$$

So in this norm the nonlinear term does not disappear. It is only in the L_2 norm that the nonlinear term disappears. The dynamic equation for the H^{-1} is then

$$(5.31) \quad \frac{d}{dt} \sum_{\kappa=1}^{\infty} \frac{|\hat{q}_\kappa|^2}{\kappa^2} = \hat{W} + \sum_{\kappa=0}^{\infty} |\hat{q}_\kappa|^2 - \kappa^2 |\hat{q}_\kappa|^2.$$

5.5.1 Equation for H^{-1} norm for hyperviscous regularization technique

For ν_6 the dynamic equation changes into

$$(5.32) \quad \frac{\partial}{\partial t} \sum_{\kappa=1}^{\infty} \frac{|\hat{p}_\kappa|^2}{\kappa^2} = \hat{W} + \sum_{\kappa=1}^{\infty} |\hat{p}_\kappa|^2 - \kappa^2 |\hat{p}_\kappa|^2 + \nu_6 \kappa^4 |\hat{p}_\kappa|^2.$$

The higher order term will again act to decrease the norm as was the case of the regularization based on the L_2 norm. However, in this case the regularization coefficient is multiplied by the H^2 norm and not the H^3 norm. This was expected as the H^{-1} norm has more to do with the large scales of the problem. So we should increase the coefficient ν_6 if the H^{-1} norm is higher than the reference level and decrease ν_6 if H^{-1} norm is too low.

5.5.2 Equation for H^{-1} norm for pseudo–parabolic technique

The results are similar to the treatment of the L_2 norm. In the end one will get the following dynamic equation for the H^{-1} norm

$$(5.33) \quad \frac{d}{dt} \sum_{\kappa=1}^{\infty} \frac{|\hat{p}_\kappa|^2}{\kappa^2} = \hat{W} + \sum_{\kappa=1}^{\infty} |\hat{p}_\kappa|^2 - \kappa^2 |\hat{p}_\kappa|^2 + \nu_{dt} \frac{d}{dt} \kappa^2 |\hat{p}_\kappa|^2.$$

But now the time derivative is in respect to the H^{-1} norm. So the dynamic equation for H^{-1} norm using this technique is similar the dynamic equation of the L_2 norm with the same technique, but everything has moved to a “lower” norm.

5.6 Adaptive adjustment of the magnitudes of the regularization terms

One can provide a fixed value ν_6 or ν_{dt} to use to find a solution to the terminal value problem. This is the standard approach. The trouble with this is that the optimal value of the regularization coefficients depends on φ and T in a non trivial manner. And by “optimal” we mean a solution to the terminal value problem that is closest in a given norm to the solution of the initial value problem. The way of measuring this is the following: start with the initial value problem, get a solution at $t = T$, use this solution $u(T)$ as

the terminal value in the backward problem. In the terminal value problem we will try to reconstruct the starting values $u(0)$ from the initial value problem. If φ has a lot of energy located at small scales, the regularization coefficient needs to be big enough to prevent that too much energy is transported into small scales. Otherwise the Fourier modes that correspond to the high wave numbers will grow very fast. In this research we will do something different, namely we will try to find the good values of the regularization coefficient ν for $0 \leq t \leq T$ given some properties of the problem. And by “good” we mean lower error in some norm at $t = 0$ than the best value of the error norm obtained with any fixed value of the regularization parameter. We will give ourselves the freedom to vary the coefficients while we solve the terminal value problem. So the magnitude of the regularization term will be allowed to change in time. This adaptation will be performed based on some information about the corresponding initial value problem, e.g. a mean or instantaneous norm of solution. Below we describe different techniques that can be employed to carry out this adaptation. See figure 5.7 for a schematic sketch of what we will attempt to do. Notice that we only have information about the solution and the regularization parameter at t^{i+1} , not t^{i-1} . This is because we are marching backwards-in-time. If we want to get information about the current time-step we have to calculate it, which is not hard but requires a “test” time step.

5.6.1 Instantaneous adaptation

Here the idea is to take a candidate value of the regularization coefficient and take one test time step and see the result. Using this method one tries to find a value of the regularization coefficient that satisfies some criteria. Here we will try and find a value of the regularization coefficients that makes the L_2 norm constant in the interval $0 \leq t \leq T$. So we want to find a value for the coefficient that solves

$$(5.34) \quad \|\hat{p}(t, \nu)\|_{\mathcal{X}} - \|\hat{u}(T)\|_{\mathcal{X}} = 0$$

where \mathcal{X} is a chosen function space. Using this estimate with the assumption that the function that we try to find the zero of depends continuously on the regularization coefficient, we can use common techniques to find the optimal value of the regularization coefficient.

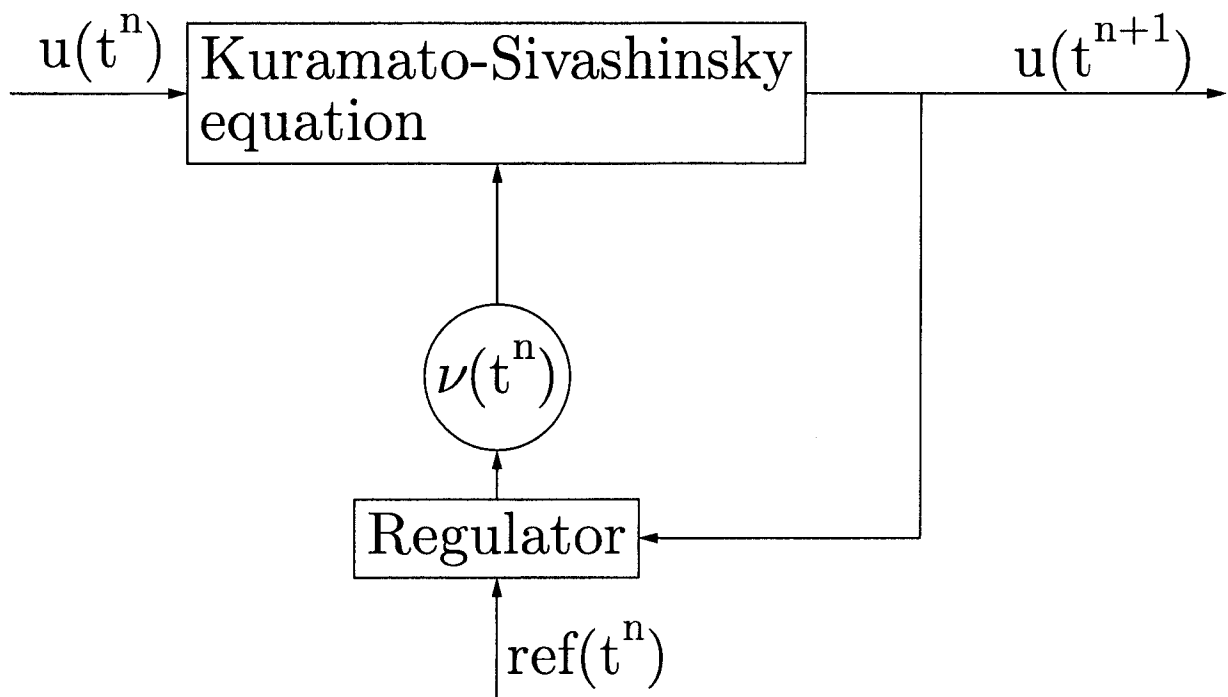


Figure 5.7: A sketch describing the concept of adaptive regularization as a feedback loop. Note that the regulator is allowed to save information from $t > t^n$.

For this research we used Newton’s method.

5.6.2 P–regulator

This idea is from control theory [25]. The idea is to adjust the coefficient based on some quantity we want to have a given value. So we want $e(t)$ to be close to zero, where $e(t)$ is defined as

$$(5.35) \quad e(t) = \|\hat{p}(t)\|_{\mathcal{X}} - \|\hat{u}(T)\|_{\mathcal{X}}$$

and \mathcal{X} is a chosen function space. The regularization coefficient ν will update based on the following algorithm

$$(5.36) \quad \nu(t^i) = \nu(t^{i+1}) + K_P \cdot e(t^{i+1}).$$

Two parameters are needed in order for this algorithm to work, namely K_P and $\nu(T)$.

5.6.3 PD–regulator

This is similar to the previous approach, but now one considers how the quantity changes in time as well. So the update algorithm to update this technique is

$$(5.37) \quad \nu(t^i) = \nu(t^{i+1}) + K_P \cdot e(t^{i+1}) + K_D \cdot \frac{de(t^{i+1})}{dt}.$$

where the time derivative of $e(t)$ is approximated by

$$(5.38) \quad \frac{de(t^i)}{dt} \approx \frac{e(t^{i+1}) - e(t^i)}{\Delta t}$$

This means that now one needs three parameters, K_D , K_P and $\nu(T)$.

5.6.4 Comparison to different adaptive schemes

We do not have any guarantee that the instantaneous adaptation will find a ν that fulfills equation 5.34 for all \hat{p} and t . If we are unable to find a solution, we will use the best candidate found. For the terminal value problem for heat equation it has been proved that the solutions will depend continuously on the amplitude of the regularization parameters [20], but for the terminal value problem of Kuramoto–Sivashinsky equation the question

is still unresolved. This means that we are not sure if there even exists a value of the amplitude that for the current solution keeps the selected norm constant. The P regulator and PD regulator will always find a new dynamic value, but in classical control theory we are worried about three issues: overshoot, adjustment time and offset. If $e(t)$ changes sign during its adjustment to zero, the overshoot is the maximum derivative after this change occurred. If $e(t)$ does not change sign, there is no overshoot. Adjustment time is the time it takes before $e(t)$ is approximately constant. The offset is the value $\lim_{t \rightarrow \infty} e(t)$.

The value of K_P will affect all three issues [25]. With increasing K_P , the overshoot will increase. However adjustment time and offset will increase. By increasing K_D , the overshoot will decrease. Adjustment time increases and the offset will increase.

We could use PID regulator, this regulator would look like

$$(5.39) \quad \nu(t^{i+1}) = \nu(t^i) + K_P \cdot e(t^i) + K_I \int_0^{t^i} e(\tau) d\tau + K_D \cdot \frac{de(t^i)}{dt}.$$

This regulator would remove the offset. The problem with this regulator is that the derivative response D would interact with integral response I and both of them would follow the proportional response P [25]. So all of them would act like a P regulator in short time windows.

Chapter 6

Results of the regularization algorithms

We will start by solving the initial value problem

$$(6.1) \quad \begin{cases} \frac{\partial \hat{u}_\kappa}{\partial t} - \hat{w}_\kappa - \kappa^2 \hat{u}_\kappa + \kappa^4 \hat{u}_\kappa = 0, & \kappa = 0, \dots, N, \quad t \in [0, T] \\ \hat{u}_\kappa(0) = \hat{\phi}_\kappa. & \kappa = 0, \dots, N \end{cases}$$

The solution \hat{u} at $t = T$ will be used as the terminal value for (3.1). To measure the error we will use three different norms namely, the L_2 norm, H^1 norm and H^{-1} norm. We will use the following truncated expressions for our calculations

$$(6.2) \quad L_2 : \frac{\|e(t)\|_{L_2}^2}{\|u(t)\|_{L_2}^2} = \frac{\sum_{\kappa=1}^N |\hat{e}_\kappa(t)|^2}{\sum_{\kappa=1}^N |\hat{u}_\kappa(t)|^2},$$

$$(6.3) \quad H^1 : \frac{\|e(t)\|_{H^1}^2}{\|u(t)\|_{H^1}^2} = \frac{\sum_{\kappa=1}^N \kappa^2 |\hat{e}_\kappa(t)|^2}{\sum_{\kappa=1}^N \kappa^2 |\hat{u}_\kappa(t)|^2},$$

$$(6.4) \quad H^{-1} : \frac{\|e(t)\|_{H^{-1}}^2}{\|u(t)\|_{H^{-1}}^2} = \frac{\sum_{\kappa=1}^N \frac{|\hat{e}_\kappa(t)|^2}{\kappa^2}}{\sum_{\kappa=1}^N \frac{|\hat{u}_\kappa(t)|^2}{\kappa^2}},$$

where $\hat{e}(t) = \hat{p}(t) - \hat{u}(t)$ and $\hat{p}(t)$ denotes the Fourier transform of the solution of the regularized problem (5.5) and \hat{u} is the Fourier transform of the solution to the initial value problem in system (6.1) at time t . For more information about the norms see sections 5.4 and 5.5. The different norms will focus on different length scales of the error. The H^{-1} norm focus on the large scales of the solution, the L_2 norm treats all length scales uniformly and the H^1 norm is focused on the smallest scales of the solution.

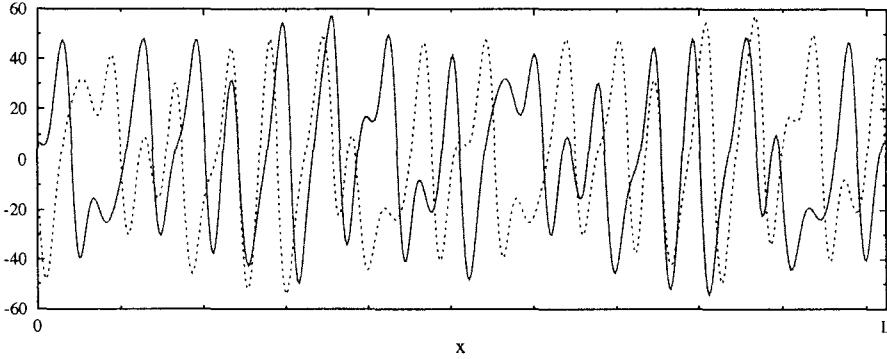


Figure 6.1: Comparison of a starting condition and the same starting condition shifted by $L/2$ in the x direction.

The trouble with using the L_2 norm is that even though one solution to the terminal value problem can have the same energy as the solution to the initial value problem, the relative error can be large. It can be larger than unity which in turn means that the zero solution is better than the solution we have obtained from the regularization technique.

For example if the solution is shifted in space a distance of $L/2$ as seen in figure 6.1, then the Fourier components will be shifted by $e^{i\pi}$. This will make the solution to have error equal to 2 in the L_2 norm. This solution should be almost as good as the original, but here we can see that the norm we are using to measure error is sensitive to shifts. We have not found a solution to this problem. The ideal measurement of error would be shift invariant. Another way to measure the error is to compare the curvature. The curvature is defined as [26]

$$(6.5) \quad k(x) = \frac{\frac{\partial^2 u}{\partial x^2}}{\left(1 + \left(\frac{\partial u}{\partial x}\right)^2\right)^{3/2}}.$$

This is important for applications in combustion. If one tries and measure the difference in curvature between two solutions, one would find that this is more sensitive to shifts. Furthermore, because it uses the second derivative of u , it will be focused on the small scales of the solution, in which regularization has a large effect. See figure 6.2 for a example of curvature of a solution on the attractor. Most calculations are done on a system with $L = 154$ and $N = 1024$ number of nodes in real space.

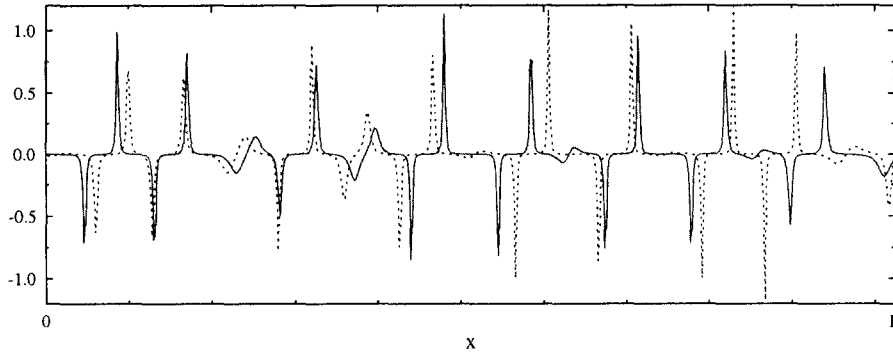


Figure 6.2: Comparison of curvature for solutions on the attractor \mathcal{A} , solid line corresponds to the starting value of the initial value problem $t = 0$, dashed line corresponds to the solution of the initial value problem at $t = T$.

6.1 Hyperviscous regularization

Generally, this regularization technique will change the form of the energy spectrum as described in section 5.3. We want to have some reference to compare with, so we solve the terminal value problem with hyperviscous regularization using a fixed value of the regularization parameter. The typical error measured in L_2 norm at different times are shown in figure 6.3. In table 6.2, one can see the result of putting different fixed value for the regularization coefficient. In the same table there appears to be a minimum at $\nu_6 = 2.7 \cdot 10^{-5}$. This value will be used as a reference for the different methods of adapting ν_6 in time. The initial state ϕ reconstructed by solving the terminal value problem (5.5) with the best fixed value of ν_6 is compared against the actual initial state in figure 6.4. The adaptive algorithm used are listed in table 6.1. Note that this reference would cause a small shift in κ_0, κ_{max} as described in section 2.3. The shift is very small for both of them, on the order of $O(10^{-3})$.

6.1.1 Regularization of the linearized Kuramoto–Sivashinsky equation

Previously we speculated that the nonlinear term would help us in stabilizing solutions to the terminal value problem. The idea was that the nonlinear term would transfer energy

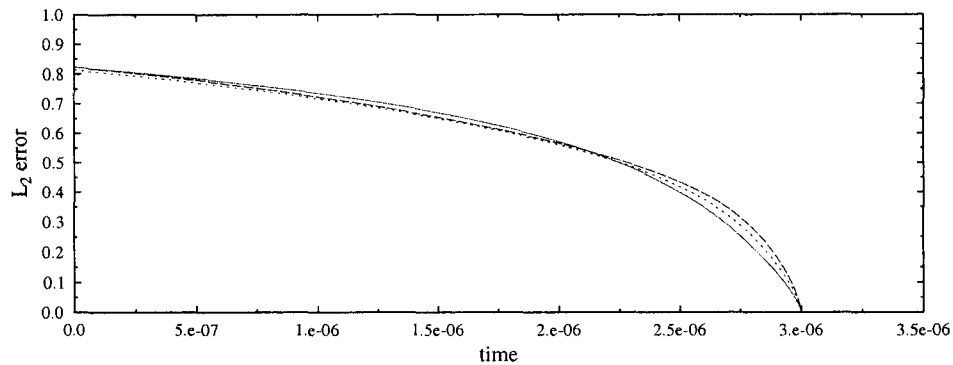


Figure 6.3: The L_2 error as a function of time T for three different values of the hyperviscous regularization parameter, (solid line) $\nu_6 = 1.8 \cdot 10^{-5}$, (dotted line) $\nu_6 = 2.7 \cdot 10^{-5}$, (dashed line) $\nu_6 = 3.5 \cdot 10^{-5}$.

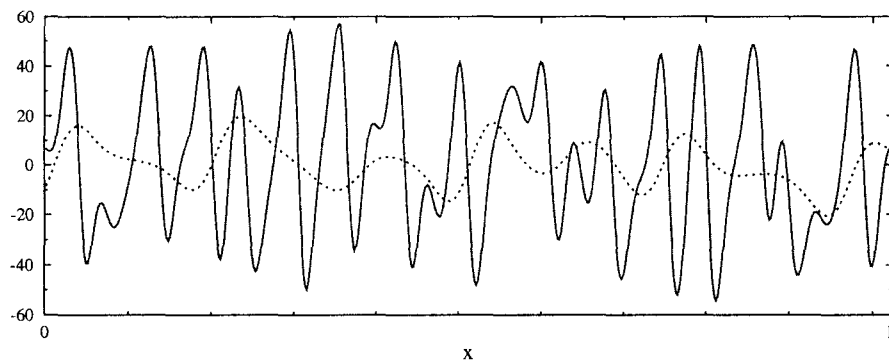


Figure 6.4: Comparison of the (solid line) the initial condition ϕ in the initial value problem (2.3) and (dashed line) the solution of the regularized terminal value problem (5.5) $p(t = 0)$ with $\nu_6 = 2.7 \cdot 10^{-5}$.

	L_2 norm	H^{-1} norm
Instantaneous	hL_2	—
P regulator	hPL_2	hPH^{-1}
PD regulator	$hPDL_2$	—

Table 6.1: Different algorithms used to regularize the solution to the terminal value problem with hyperviscous regularization technique

ν_6	$\ e(0)\ _{L_2}/\ u(0)\ _{L_2}$
$6.7 \cdot 10^{-8}$	∞
$8.7 \cdot 10^{-6}$	1.99
$1.8 \cdot 10^{-5}$	0.82
$2.7 \cdot 10^{-5}$	0.81
$3.5 \cdot 10^{-5}$	0.82
$4.5 \cdot 10^{-5}$	0.83
$5.3 \cdot 10^{-5}$	0.86
$6.2 \cdot 10^{-5}$	0.87
$7.1 \cdot 10^{-5}$	0.87
$8 \cdot 10^{-5}$	0.87

Table 6.2: The relative L_2 error (6.2) at $t = 0$ for fixed values of the regularization parameter

from the small scales of the solution into the larger scales of the solution. And since in the solution to the terminal value problem energy is injected into the small scales and dissipated at the large scales this would prevent the energy in the small scales from getting too big. In figure 6.5, we can see the result of removing the nonlinear term. This means that the linearized problem we will solve is

$$(6.6) \quad \left\{ \begin{array}{l} \frac{\partial p}{\partial t} + \frac{\partial^2 p}{\partial x^2} + \frac{\partial^4 p}{\partial x^4} + \nu_6 \mathcal{B}p = 0, \quad x \in [0, L], \quad t \in [0, T], \\ \frac{\partial^i p(0, t)}{\partial x^i} = \frac{\partial^i p(L, t)}{\partial x^i}, \quad t \in [0, T], \quad i = 0, \dots, 3, \\ p(x, T) = \varphi, \quad x \in [0, L]. \end{array} \right.$$

Note that stabilizing the linearized Kuramoto–Sivashinsky equation requires a smaller amplitude of the coefficient in front of the regularization term, and it is also more accurate. Also note that the linearized Kuramoto–Sivashinsky equation does not have a attractor.

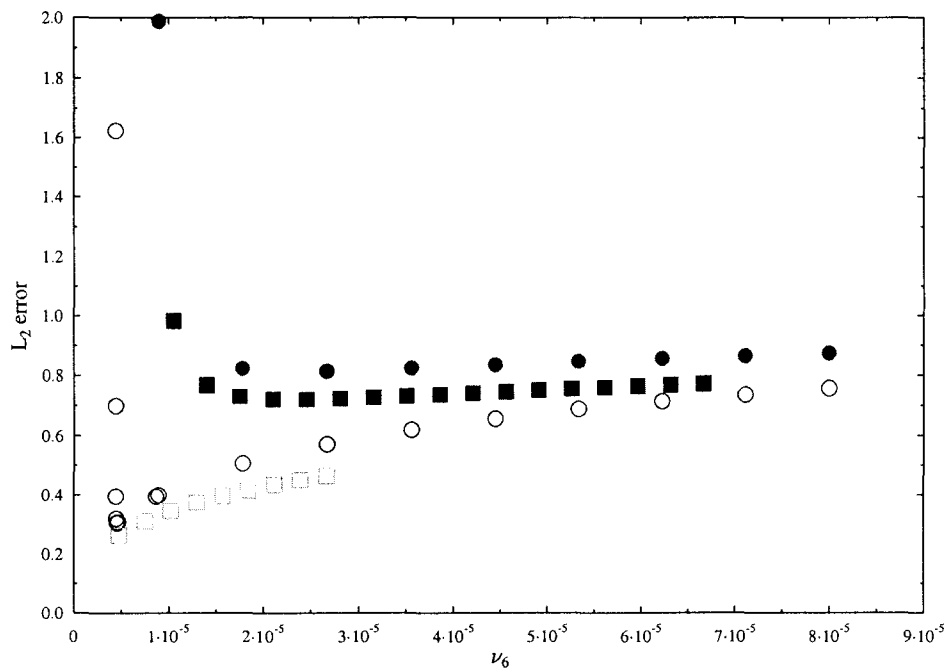


Figure 6.5: The relative L_2 error (6.2) at $t = 0$ for different fixed values of the hyperviscous regularization parameter ν_6 . \circ are the solutions for the linearized terminal value problem, \bullet are the solutions for the full terminal value problem $L = 154$, \blacksquare are for solutions with $L = 49$ and \square is for the linearized terminal value problem at the same L . The normalized time \tilde{T} is the same for all plots.

To make the comparison we use the same initial condition to solve both the initial value problem for the linearized and the full equation. So the two terminal value problem will have different terminal values.

It seems that the linearized problem requires a lower value of the regularization parameter, which was not expected. This is probably because we do not know the exact role of the nonlinear term in the Kuramoto–Sivashinsky equation. It is believed that it works in the same way as the nonlinear term in Navier Stokes, but in section 2.3 we saw that the standard argument for the energy cascade does not hold up for scrutiny. So probably we may not have transfer of energy from small to large scales. Another effect could be that in the linearized problem one starts with less energy in the small scales and that would render the solution to the terminal value problem less likely to have Fourier modes with large coefficients. This would make the non linear problem harder rather than easier to regularize. Another factor is that we are not solving the two problems with the same terminal condition. We are solving the full and the linearized Kuramoto–Sivashinsky problem with the same initial value problem to get the terminal value. In figure 6.6 we can see the difference in the energy spectrum function for the terminal value between (6.6) and (3.1). The terminal value for the full Kuramoto–Sivashinsky equation has more small scale features than the terminal value for the linearized Kuramoto–Sivashinsky equation.

In figure 6.5 we can see the effect of changing L , on the amount of regularization needed to stabilize the backward run. With increasing L a larger value of the regularization coefficient is required to stabilize the terminal value problem of the Kuramoto–Sivashinsky equation. If L is small, then the solution to the regularized terminal value problem will be slightly more accurate. This is consistent with the idea that with increasing L we get more chaotic behaviour of the solutions.

Because the Kuramoto–Sivashinsky equation has qualitatively different properties for different L [27], we will not analyze solutions at very small value of L . The reason that for a very small value of L the attractor is a fixed point or the zero solution. We want to solve a chaotic problem with multiscale behaviour and for small values L the solution to the Kuramoto–Sivashinsky equation does not have such properties.

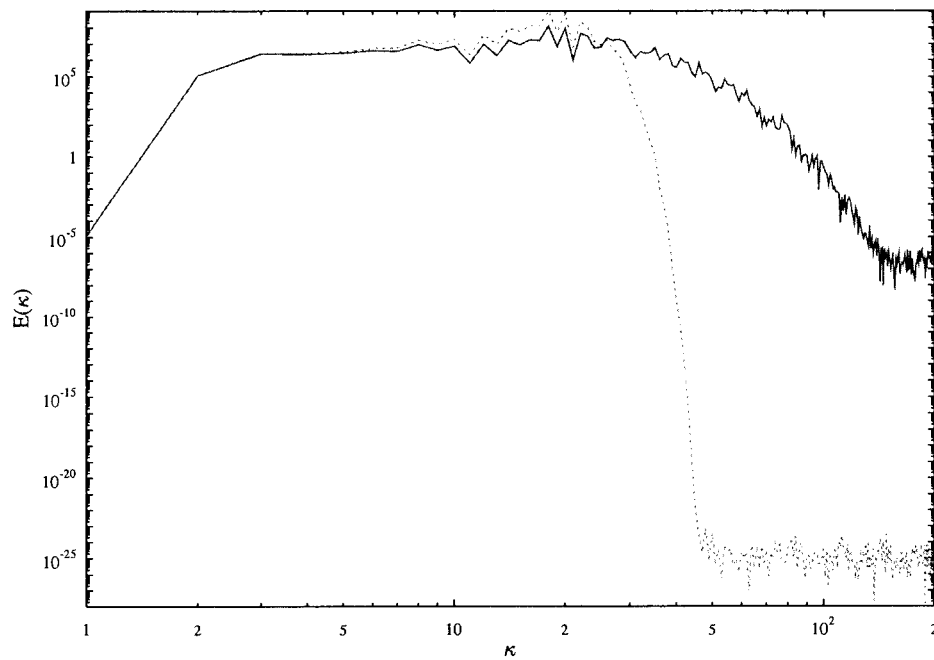


Figure 6.6: Energy spectrum for the terminal value problems (5.5) and (6.6) at $t = 0$, (solid line) the full Kuramoto–Sivashinsky equation (5.5), (dashed line) the linearized Kuramoto–Sivashinsky equation (6.6). Both with $L = 49$.

6.1.2 Instantaneous adaptation

This section is about using Newton's method to choose a value of ν_6 in which the L_2 norm of the solution constant. The problem is that this method is very unstable. It does not always work, as can be seen in figure 6.7, it may converge to a different value of the L_2 norm. In this figure the algorithm converged to a solution that gave the L_2 norm an approximate value of 4200, instead of the required 3160. This is of course not a solution of the following equation

$$(6.7) \quad \|p(t)\|_{L_2} - \|u(T)\|_{L_2} = 0.$$

but a local minimum of the left hand side. The time history of the L_2 error norm and the solution obtained at $t = 0$ are shown in figure 6.8 and 6.9.

6.1.3 L_2 norm with the P-regulator

Here we will use the L_2 norm as a reference level. The L_2 norm is almost constant when the initial value problem (6.1) has reached the attractor. From the plots of the energy obtained during the solution of initial value problem starting from sine wave, we can see that the energy variation is a couple of percent of the total energy when the attractor is reached, see figure 5.1. Thus, first of all, we need to make sure that the start of the initial value problem is on the attractor. All calculations are made with periodic boundary conditions.

When the energy is stable we conclude that the solution has reached the attractor and can be used as a terminal condition for the backwards run. So now we can start the backwards run with the forwards run final data. The L_2 norm is defined by via Parseval's theorem:

$$(6.8) \quad \|u\|_{L_2}^2 = \int_0^L u^2 dx \simeq \sum_{\kappa=0}^N |\hat{u}_\kappa|^2.$$

The coefficient ν_6 will update based on the following algorithm (see section 5.6.2)

$$(6.9) \quad \nu_6(t^i) = \nu_6(t^{i+1}) + K_P(\|p(t^{i+1})\|_{L_2} - \|u(T)\|_{L_2}).$$

The reference is taken from the solution of the initial value problem at $t = T$. If the energy is too large, one must increase ν_6 and if the energy is too small, one must decrease ν_6 . So we need two elements to make the algorithm work, K_P and a starting value for ν_6 :

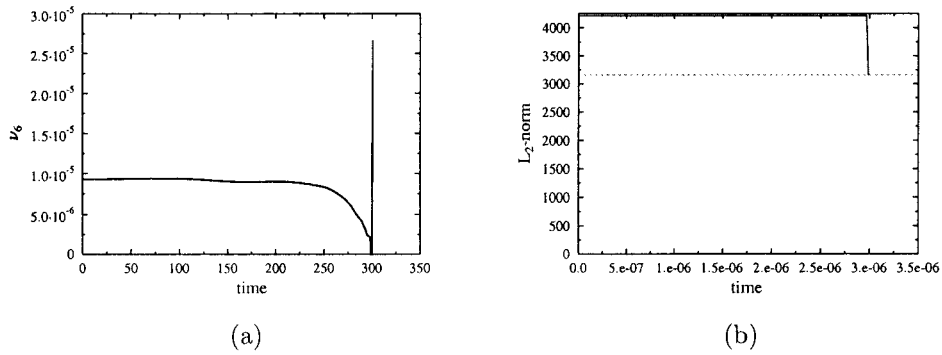


Figure 6.7: (CASE hL_2) Time histories of (a) the regularization parameter ν_6 and (b) (solid line) L_2 norm of the solution using instantaneous adaptation to control the L_2 norm with Newtons method, (dotted line) reference level for the L_2 norm.

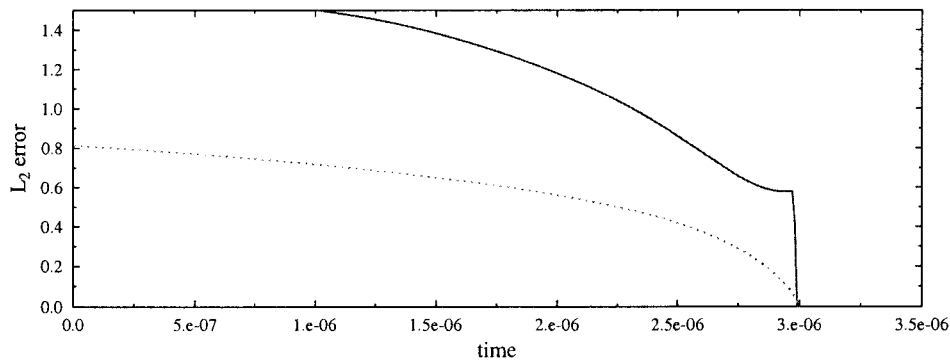


Figure 6.8: (CASE hL_2) L_2 error norm over the window $[0, T]$, solid line is for the instantaneous adaptation to control the L_2 norm, dashed line is for a fixed value of ν_6

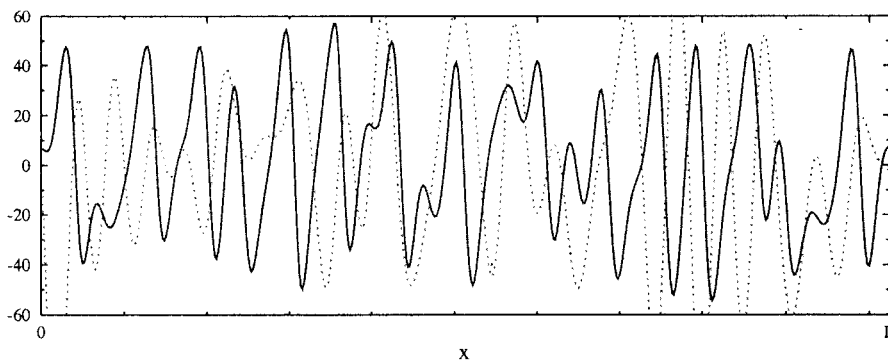


Figure 6.9: (CASE hL_2) Comparison of the (solid line) the initial condition ϕ in the initial value problem (6.1) and (dashed line) the solution of the regularized terminal value problem (5.5) $p(t = 0)$.

- There are a lot of different candidates for the starting value of ν_6 . One is the value that makes the value of the L_2 norm the same as in the first and second time steps. This value is usually very low. The second choice could be the value that ν_6 is equal to when $t = 0$. This means that one requires a first run to decide the starting value of ν_6 . There is no guarantee that this limit is independent of the candidate in the first run. This choice usually results in ν_6 attaining a low value after 10 time steps and then we have to increase it to compensate for the large amount of energy in the solution to the perturbed terminal value problem. The last one is picking a good candidate from experiments using a fixed value of ν_6 for the whole calculation of the perturbed terminal value problem. The first method will give a very low starting value of ν_6 , the second method will require a lot of numerical experiments to find the starting value. We choose a starting value from the fixed values already tested. The value used is $4 \cdot 10^{-3}$.
- The K_P parameter is used to control the proportional response to the error. We are mainly interested in two things, namely the adjustment time and overshoot. We want the adjustment time to be as short as possible and that the overshoot is as small as possible. A very large value of K_P will make the backward solution unstable. A large value of K_P will decrease the adjustment time, but increase the overshoot. A too small value of K_P will cause the change in ν_6 to be very small and thereby making very little change from using a fixed value. By experiment we observe that the L_2 norm will start by decreasing and later there will be a sharp overshoot. We will adjust K_P so that the sharp overshoot will happen after T , this means that we will not observe it during the solution to the terminal value solution.

In figures 6.10–6.12 we can see the effect of choosing K_P too large. The amplitude of ν_6 changes very quickly and the offset is very large. The L_2 norm is too high in the solution obtained. On the other hand with a smaller value of K_P we get the solution at $t = 0$ corresponding to figure 6.15. In figure 6.13 we can see that the K_P regulator has now lower amplitude of the regularization coefficient during the backward march. It seems that the L_2 norm error increases very fast if ν_6 are changed rapidly. Results shown in figure

6.10–6.12 and 6.13–6.15 indicate that reconstruction in the second case is better, even though the regularization did not quite stabilize the L_2 norm.

6.1.4 L_2 norm with the PD -regulator

Because of the overshoot in the P -regulator, one can try and use a PD -regulator to limit this effect. The regularization coefficient $\nu_6(t)$ will be determined the following way

$$(6.10) \quad \nu_6(t^i) = \nu_6(t^{i+1}) + P(\|p(t^{i+1})\|_{L_2} - \|u(T)\|_{L_2}) + D \frac{d(\|p(t^{i+1})\|_{L_2} - \|u(T)\|_{L_2})}{dt},$$

where the time derivative is approximated using the forward difference,

$$(6.11) \quad \frac{d\|p(t^i)\|_{L_2} - \|u(T)\|_{L_2}}{dt} \approx \frac{\|p(t^{i+1})\|_{L_2} - \|p(t^i)\|_{L_2}}{\Delta t}.$$

For this algorithm to work in determining the regularization coefficient one needs three elements:

- There are a lot of different candidates for the starting value of ν_6 . One is the value that makes the L_2 norm constant in that time step. This value is usually very low. The second choice could be the value that ν_6 tends towards when $t \rightarrow T$. This choice usually results in that ν_6 attains a low value after 10 time steps and then we have to increase it to compensate for the large amount of energy in the solution to the perturbed terminal value problem. The last one is picking a good candidate from experiments using a fixed value of ν_6 for the whole calculation of the perturbed terminal value problem. We will choose the starting value in the same way that we did in the P -regulator i. e., $\nu_6 = 4 \cdot 10^{-3}$.
- The K_P parameter is used to control the proportional response to the error. We start by setting K_D to zero and then increase K_P until the perturbed system is stable. We are interested in two things, namely the adjustment time and overshoot. We want the overshoot to be as small as possible. With the PD -regulator we have the possibility of increasing K_P and use K_D to decrease the size of the overshoot.
- The K_D parameter is used to control the feedback from the derivative of the error. This parameter will decrease the overshoot and increase the adjustment time. For

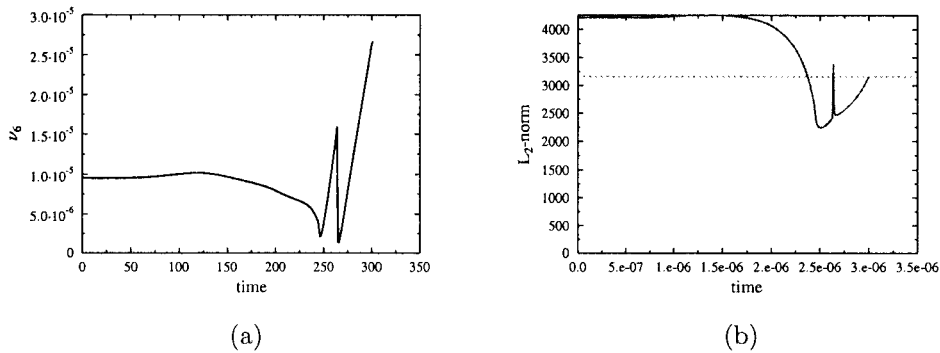


Figure 6.10: (CASE hPL_2) Time histories of (a) the regularization parameter ν_6 and (b) (solid line) L_2 norm of the solution using P regulator to control the L_2 norm with $P = 7 \cdot 10^{-8}$, (dotted line) reference level for the L_2 norm.

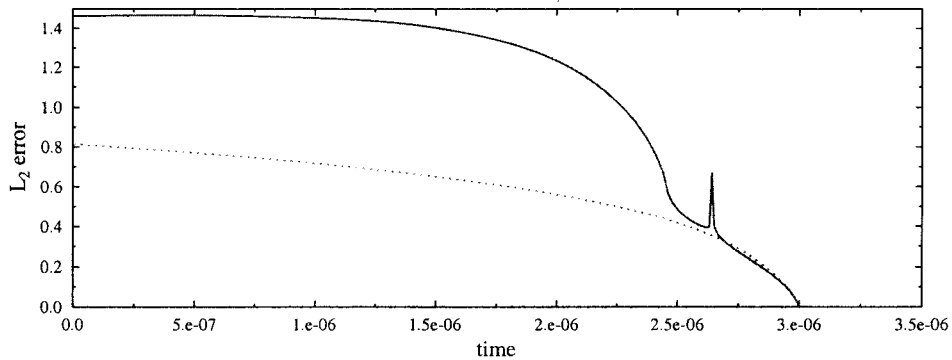


Figure 6.11: (CASE hPL_2) L_2 error norm over the window $[0, T]$, solid line is for the P regulator to control the L_2 norm, dashed line is for a fixed value of ν_6

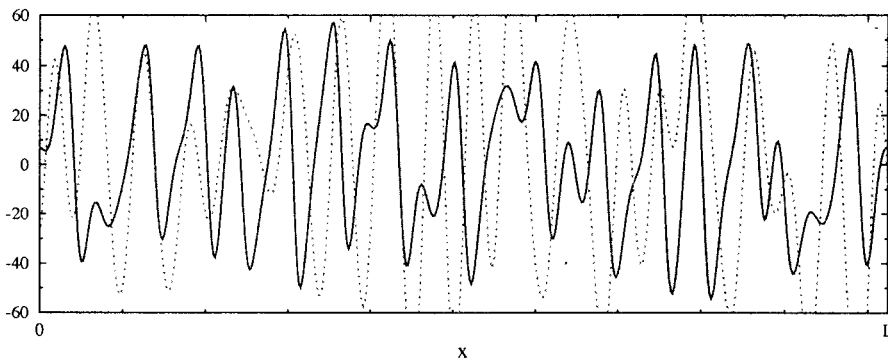


Figure 6.12: (CASE hPL_2) Comparison of the (solid line) the initial condition ϕ in the initial value problem (6.1) and (dashed line) the solution of the regularized terminal value problem (5.5) $p(t = 0)$.

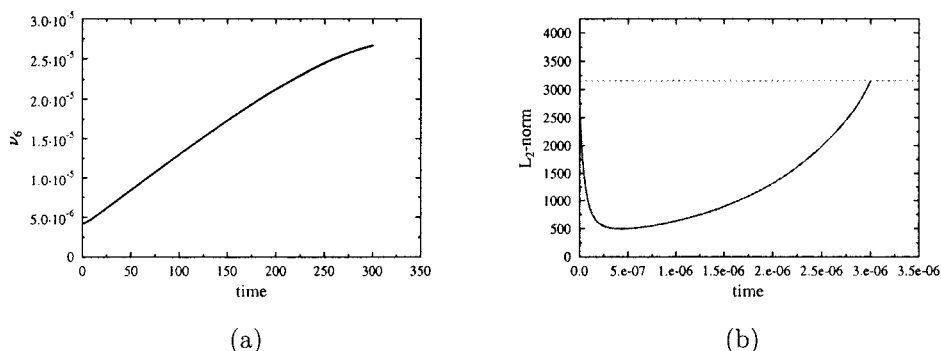


Figure 6.13: (CASE hPL_2) Time histories of (a) the regularization parameter ν_6 and (b) (solid line) L_2 norm of the solution using P regulator to control the L_2 norm with $P = 5 \cdot 10^{-9}$, (dotted line) reference level for the L_2 norm.

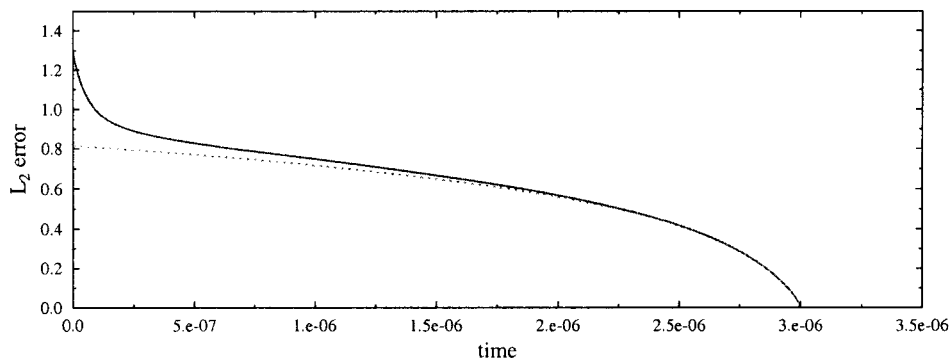


Figure 6.14: (CASE hPL_2) L_2 error norm over the window $[0, T]$, solid line is for the P regulator to control the L_2 norm, dashed line is for a fixed value of ν_6

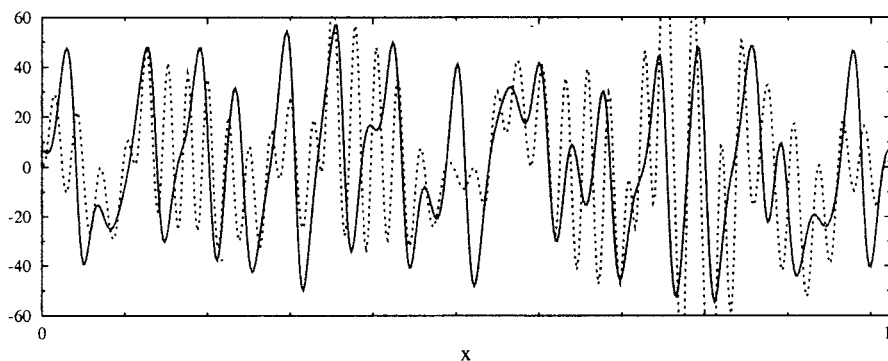


Figure 6.15: (CASE hPL_2) Comparison of the (solid line) the initial condition ϕ in the initial value problem (6.1) and (dashed line) the solution of the regularized terminal value problem (5.5) $p(t = 0)$.

a large value of K_D this algorithm to choose ν_6 makes the L_2 norm of solution to regularized terminal value problem go towards infinity. This will be the last parameter we will set and it will be as large as possible to decrease the overshoot and still be stable.

In figure 6.16, we can see the changing value of ν_6 during the solution of the terminal value problem. The coefficient ν_6 starts at $4 \cdot 10^{-3}$, this is the optimal value found for the perturbed terminal value problem with a fixed ν_6 . Then it decreases rapidly before settling into a final value close to $1.5 \cdot 10^{-3}$. From the plot of the L_2 norm in figure 6.16, we can see that the PD -regulator does a good job at keeping energy at the reference level. However the problem is that the dip that the energy will take during the first 50 time steps. This dip will cause the error measured in the L_2 norm to increase very fast. This limits the use of this regularization strategy since we can choose a fixed value of ν_6 that has a smaller L_2 error, see figure 6.17. So even though we manage to regulate the L_2 norm better, we did not find a better choice of the amplitude coefficients than a fixed value of ν_6 .

6.1.5 H^{-1} norm with P -regulator

The idea behind using the H^{-1} norm as a reference level is that this norm is more focused on the large scales of the problem and therefore could be less affected by noise. Generally, it seems that this norm is lagging in time in comparison with the L_2 norm. In figure 6.21 one can see that the solution has retained the large scales properties. However the solution has less energy and almost all the peaks that the solution to the original initial value problem has are not present in the backward march. If we look at figure 6.19, the energy is decreasing during the solution to the terminal value problem. The reason is that ν_6 is too large. This follows from that when the time t is close to T , the H^{-1} norm of the solution to the terminal value problem is small, so the P -regulator will try to decrease ν_6 . Unfortunately, it decreases the magnitude of the regularization coefficient too much and the solution to the terminal value problem will be given a sudden peak of energy. But here K_P is again chosen in such a way that this will happen after $t = 0$.

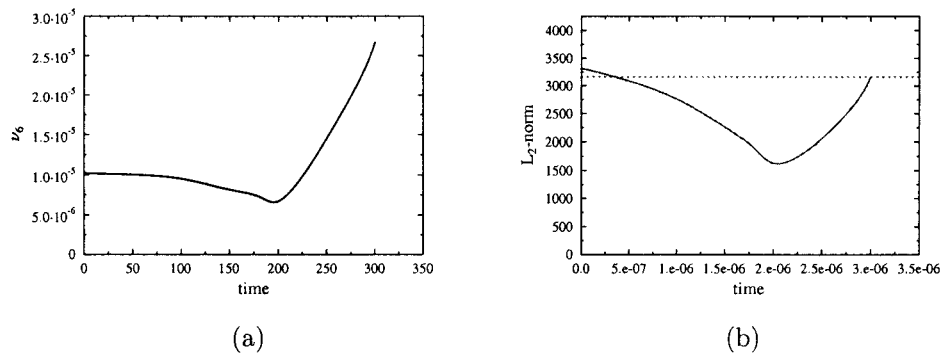


Figure 6.16: (CASE $hPDL_2$) Time histories of (a) the regularization parameter ν_6 and (b) (solid line) L_2 norm of the solution using PD regulator to control the L_2 norm with $P = 7 \cdot 10^{-9}$, $D = 5 \cdot 10^{-14}$, (dotted line) reference level for the L_2 norm.

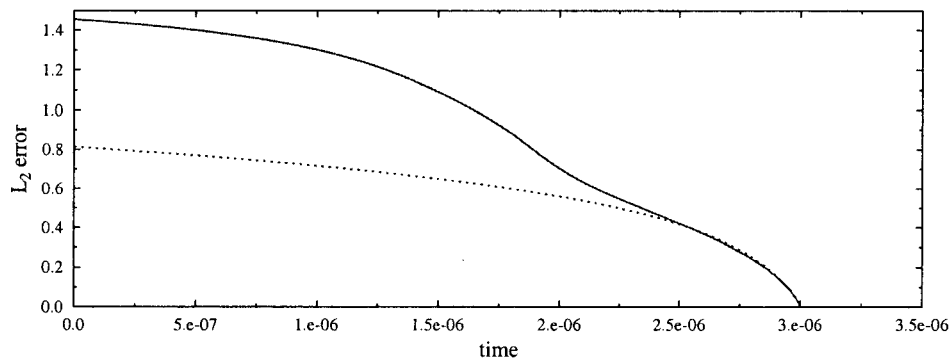


Figure 6.17: (CASE $hPDL_2$) L_2 error norm over the window $[0, T]$, solid line is for the PD regulator to control the L_2 norm, dashed line is for a fixed value of ν_6

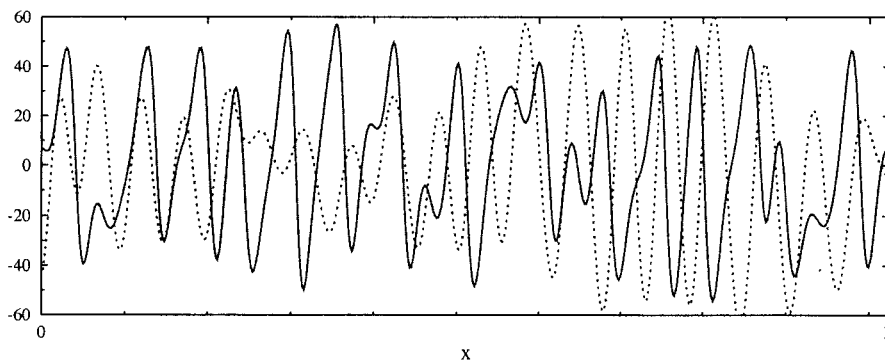


Figure 6.18: (CASE $hPDL_2$) Comparison of the (solid line) the initial condition ϕ in the initial value problem (6.1) and (dashed line) the solution of the regularized terminal value problem (5.5) $p(t = 0)$.

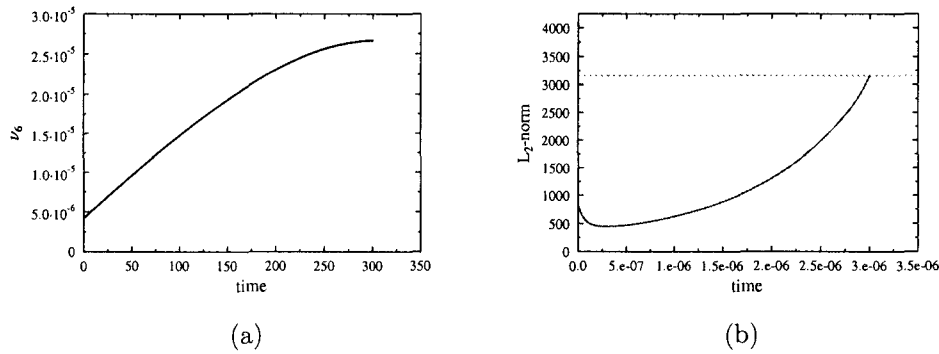


Figure 6.19: (CASE hPH^{-1}) Time histories of (a) the regularization parameter ν_6 and (b) (solid line) L_2 norm of the solution using P regulator to control the H^{-1} norm with $P = 3 \cdot 10^{-11}$, (dotted line) reference level for the L_2 norm.

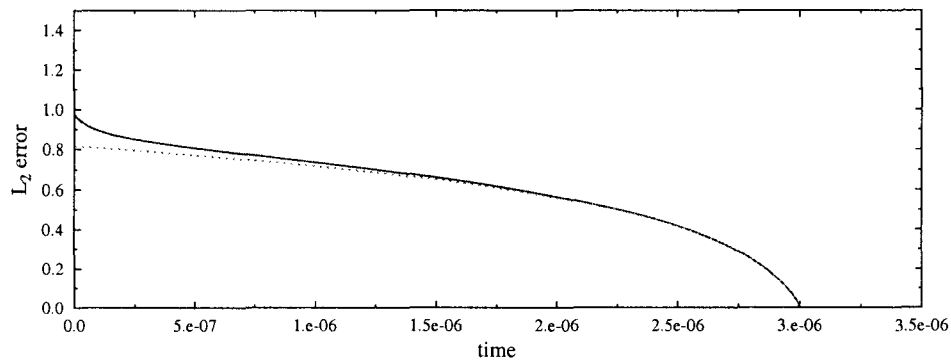


Figure 6.20: (CASE hPH^{-1}) L_2 error norm over the window $[0, T]$, solid line is for the P regulator to control the H norm, dashed line is for a fixed value of ν_6

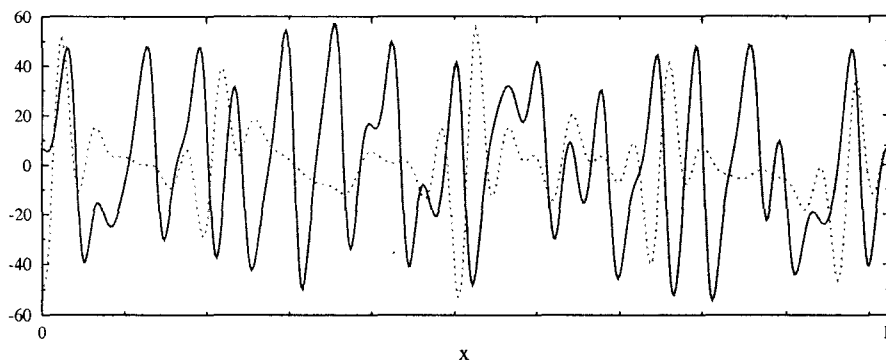


Figure 6.21: (CASE hPH^{-1}) Comparison of the (solid line) the initial condition ϕ in the initial value problem (6.1) and (dashed line) the solution of the regularized terminal value problem (5.5) $p(t = 0)$.

6.2 Pseudo–parabolic regularization

This regularization technique will not change the form of the energy spectrum as noticeably as the hyperviscous regularization does. This means that we hope that this regularization technique works better than the previous one. As in the previous section we want to have some reference to compare against. We will solve equation (3.1) with a pseudo–parabolic term added with a fixed magnitude of ν_{dt} . The error measured in the L_2 norm at $t = 0$ is in table 6.4. The pseudo–parabolic regularization will be less dependent on variations of the magnitude of the regularization coefficient than the hyperviscous regularization technique. For a typical error measured in the L_2 norm at different times look at figure 6.22. In figure 6.24, one can see that there is a minimum of the error at $t = 0$ when the regularization coefficient is $4.4 \cdot 10^{-6}$. This value will be used as a reference for the different algorithms of choosing a time dynamic ν_{dt} . The initial state ϕ reconstructed by solving the terminal value problem (5.5) with the best fixed value of ν_{dt} is compared against the actual initial state in figure 6.23.

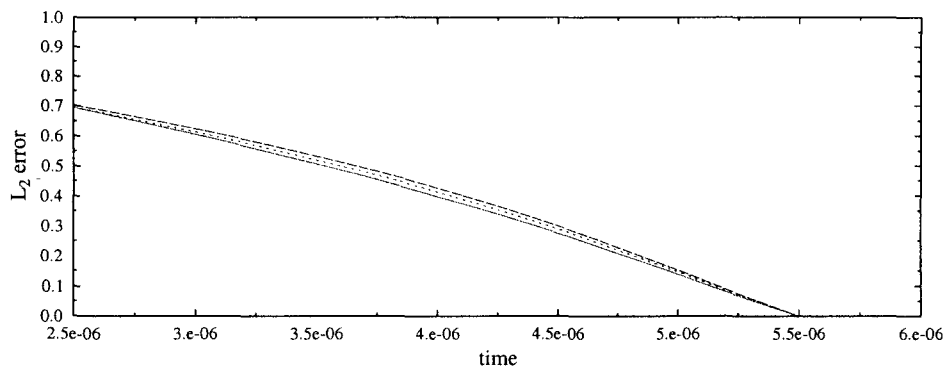
	L_2 norm	H^{-1} norm
Instantaneous	p IL_2	—
P regulator	p PL_2	p PH^{-1}
PD regulator	PDL_2	—

Table 6.3: Different algorithms used to regularize the solution to the terminal value problem with the pseudo–parabolic regularization technique.

6.2.1 Regularization of the linearized Kuramoto–Sivashinsky equation

In figure 6.24 we can see the result of removing the nonlinear term. The results are similar to the ones we have from the hyperviscous regularization 6.1.1. However, the difference between linearized Kuramoto–Sivashinsky equation and the full Kuramoto–Sivashinsky equation is large than in the case using hyperviscous regularization, which adds further evidence that the effect of the nonlinear term in the backward Kuramoto–Sivashinsky

ν_{dt}	$\ e(0)\ _{L_2}/\ u(0)\ _{L_2}$
$3.9 \cdot 10^{-21}$	∞
$5.3 \cdot 10^{-19}$	7.55
$1.0 \cdot 10^{-18}$	0.91
$1.6 \cdot 10^{-18}$	0.72
$2.2 \cdot 10^{-18}$	0.70
$2.7 \cdot 10^{-18}$	0.70
$3.3 \cdot 10^{-18}$	0.70
$3.8 \cdot 10^{-18}$	0.71
$4.3 \cdot 10^{-18}$	0.72
$4.8 \cdot 10^{-18}$	0.73

Table 6.4: The error at $t = 0$ for fixed values of the regularization parameterFigure 6.22: The L_2 error as a function of time T for three different values of the pseudo-parabolic regularization parameter, (solid line) $2.2 \cdot 10^{-18}$, (dotted line) $2.7 \cdot 10^{-18}$, (dashed line) $3.3 \cdot 10^{-18}$.

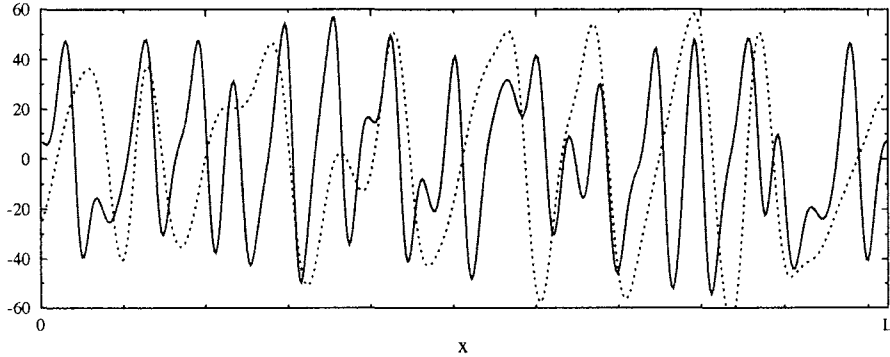


Figure 6.23: Comparison of the (solid line) the initial condition ϕ in the initial value problem (2.3) and (dashed line) the solution of the regularized terminal value problem (5.5) $p(t = 0)$ with $\nu_{dt} = 2.7 \cdot 10^{-18}$.

equation is far from clear.

6.2.2 Instantaneous adaptation

Using Newton's method to find a solution to equation (5.34) with \mathcal{X} is taken as L_2 is not straight forward. There is a risk that the algorithm will not converge. If it does converge, we can see, in figure 6.25, that it does a good job at keeping the L_2 norm constant. However it did this by making the amplitude of ν_{dt} very large (on the order of 10^8) which means that during the backward run, the following is approximately true

$$(6.12) \quad \frac{d}{dt} \sum_{\kappa=1}^{\infty} \kappa^4 |\hat{p}_{\kappa}|^2 = 0.$$

This will cause most of the Fourier modes to remain unchanged when we solve the terminal value problem. So it is as if we are using the terminal value to approximate the initial value. Of course this not a good strategy to solve our problem.

6.2.3 L_2 norm with P -regulator

Here as in the case with hyperviscous regularization technique with the P -regulator, see section 6.1.3, we will update the amplitude of the regularization coefficient ν_{dt} with the

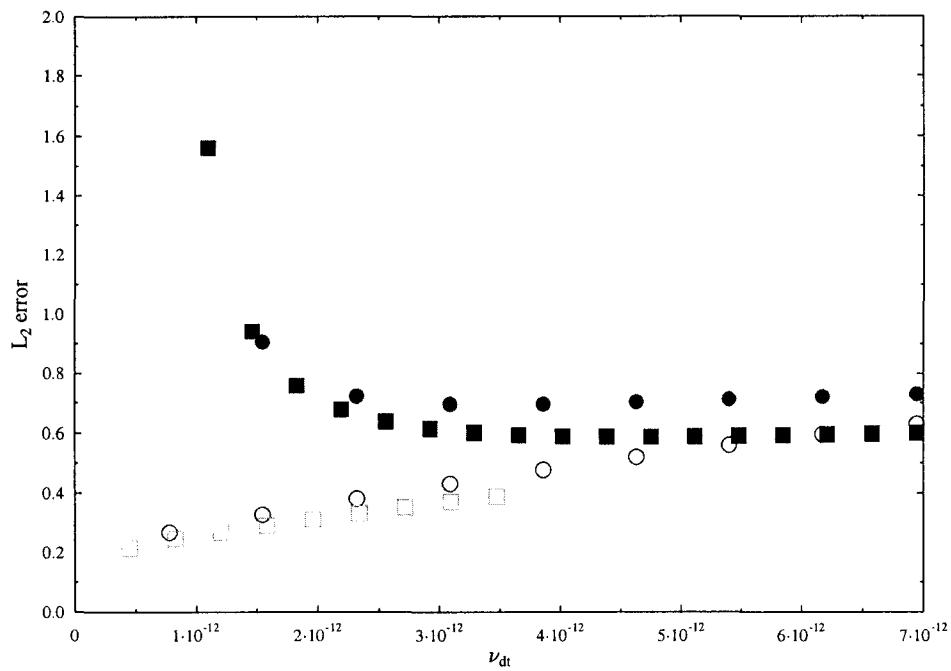


Figure 6.24: The relative L_2 error (6.2) at $t = 0$ for different fixed values of the hyperviscous regularization parameter ν_6 . \circ are the solutions for the linearized terminal value problem, \bullet are the solutions for the full terminal value problem $L = 154$, \blacksquare are for solutions with $L = 49$ and \square is for the linearized terminal value problem at the same L . The normalized time \tilde{T} is the same for all plots.

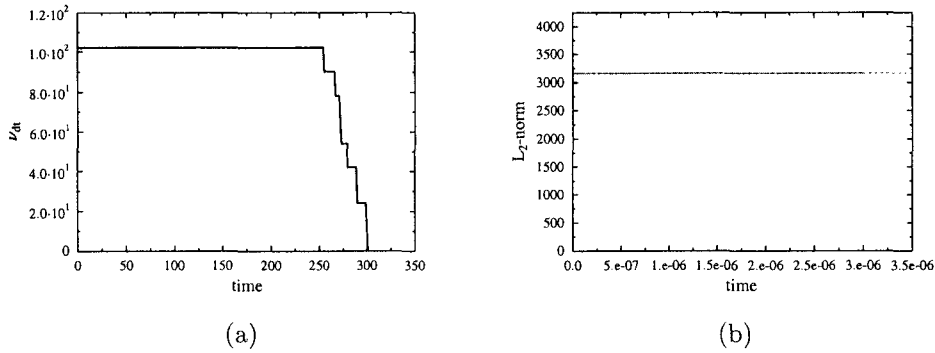


Figure 6.25: (CASE pIL_2) Time histories of (a) the regularization parameter ν_{dt} and (b) (solid line) L_2 norm of the solution using instantaneous adaptation to control the L_2 norm with Newtons method, (dotted line) reference level for the L_2 norm.

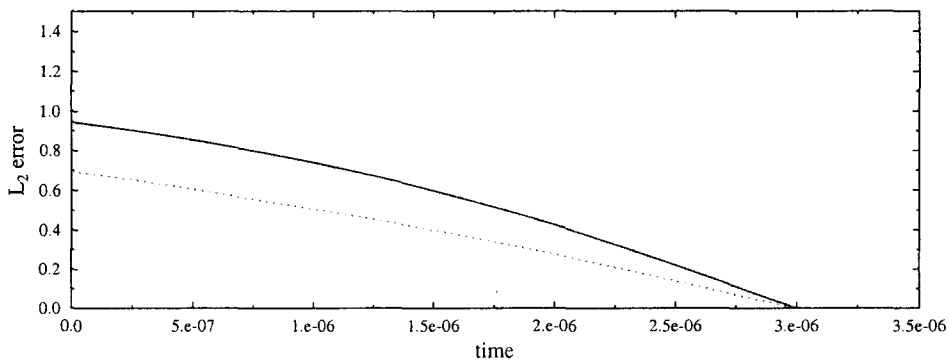


Figure 6.26: (CASE pIL_2) L_2 error norm over the window $[0, T]$, solid line is for the instantaneous adaptation to control the L_2 norm, dashed line is for a fixed value of ν_{dt}

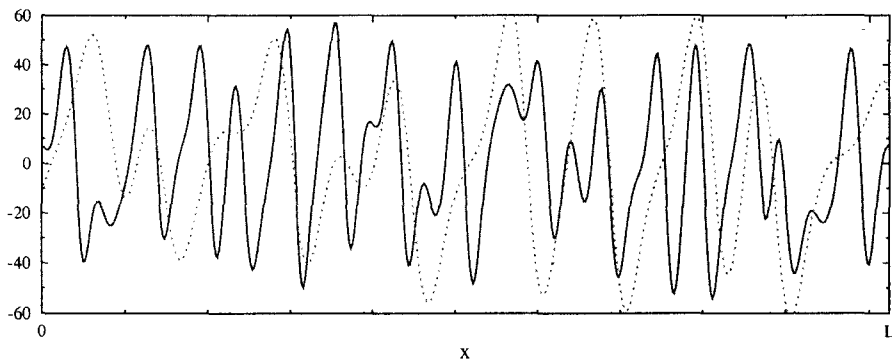


Figure 6.27: (CASE pIL_2) Comparison of the (solid line) the initial condition ϕ in the initial value problem (6.1) and (dashed line) the solution of the regularized terminal value problem (5.5) $p(t = 0)$.

following algorithm

$$(6.13) \quad \nu_{dt}(t^i) = \nu_{dt}(t^{i+1}) + K_P(\|p(t^{i+1})\|_{L_2} - \|u(T)\|_{L_2}).$$

The reference is taken from the solution of the initial value problem at $t = T$. If the energy is too large, one must increase ν_{dt} and if the energy is too small, one must decrease ν_{dt} to let more energy into the solution of the terminal value problem. So we need two elements to make the algorithm work, K_P and a starting value for ν_{dt} :

- Here we choose again a starting value from the fixed values already tested. The value used is $3.1 \cdot 10^{-12}$.
- In choosing K_P , we are mainly interested in two properties, namely the adjustment time and overshoot. Using the pseudo-parabolic regularization technique we do not see the very sharp overshoot peak. However, if K_P is chosen to a large value, we will see a very big offset from the reference value, see figure 6.28. If K_P is slightly larger the solution to the terminal value problem will have much more energy than the reference level. K_P is chosen to $2 \cdot 10^{-16}$

The results are shown in figure 6.33. This method will produce a better solution than the hyperviscous technique, but using a fixed value of the amplitude of the regularization coefficients, for example $4.4 \cdot 10^{-6}$, will still produce a better result, see figure 6.32.

6.2.4 L_2 norm with PD -regulator

We attempt to find a better algorithm to update ν_{dt} by using a PD regulator. The algorithm to determine the value of the regularization coefficient is the same as in section 6.1.4, namely,

$$(6.14) \quad \nu_{dt}(t^i) = \nu_{dt}(t^{i+1}) + K_P(\|p(t^{i+1})\|_{L_2} - \|u(T)\|_{L_2}) + D \frac{d(\|p(t^{i+1})\|_{L_2} - \|u(T)\|_{L_2})}{dt},$$

where the time derivative is approximated using the forward difference

$$(6.15) \quad \frac{d\|p(t^i)\|_{L_2} - \|u(T)\|_{L_2}}{dt} \approx \frac{\|p(t^{i+1})\|_{L_2} - \|p(t^i)\|_{L_2}}{\Delta t}.$$

For this algorithm to work in determining the regularization coefficient one needs three elements:

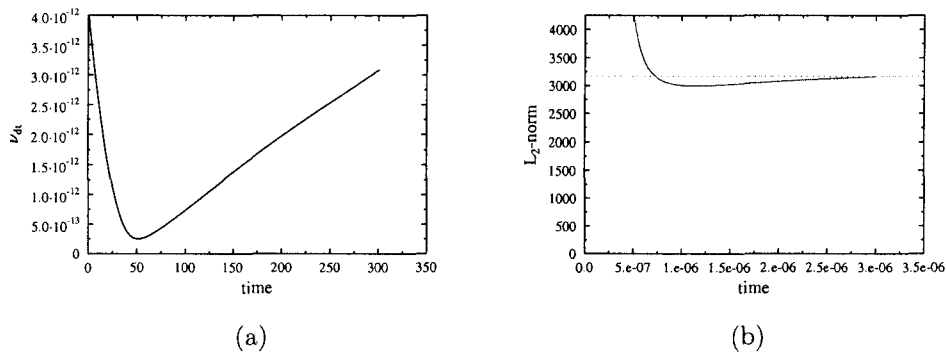


Figure 6.28: (CASE pPL_2) Time histories of (a) the regularization parameter ν_{dt} and (b) (solid line) L_2 norm of the solution using P regulator to control the L_2 norm with $P = 2 \cdot 10^{-11}$, (dotted line) reference level for the L_2 norm.

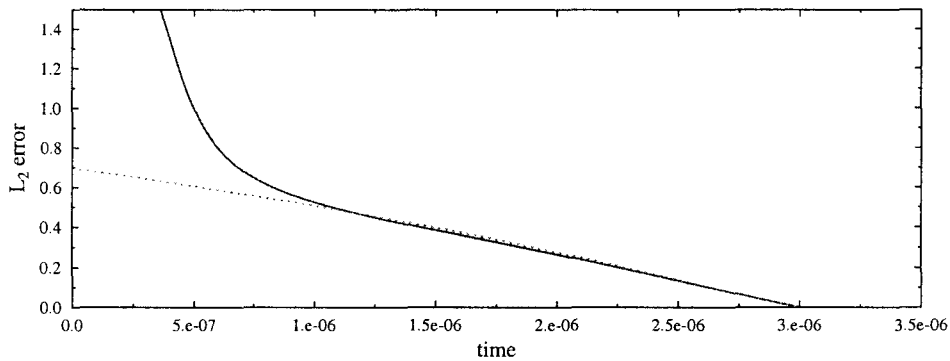


Figure 6.29: (CASE pPL_2) L_2 error norm over the window $[0, T]$, solid line is for the P regulator to control the L_2 norm, dashed line is for a fixed value of ν_{dt}

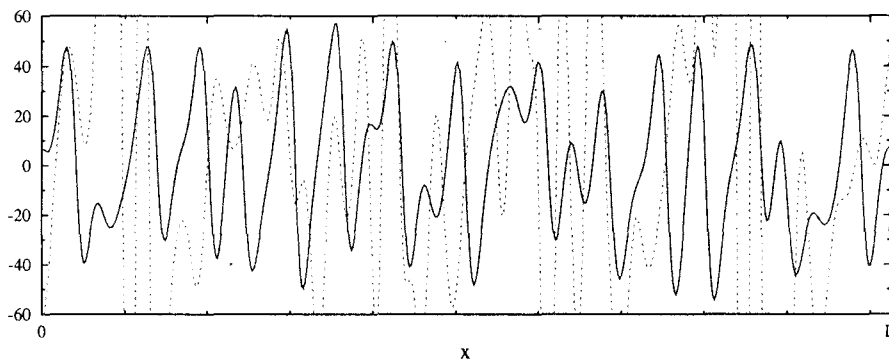


Figure 6.30: (CASE pPL_2) Comparison of the (solid line) the initial condition ϕ in the initial value problem (6.1) and (dashed line) the solution of the regularized terminal value problem (5.5) $p(t = 0)$.

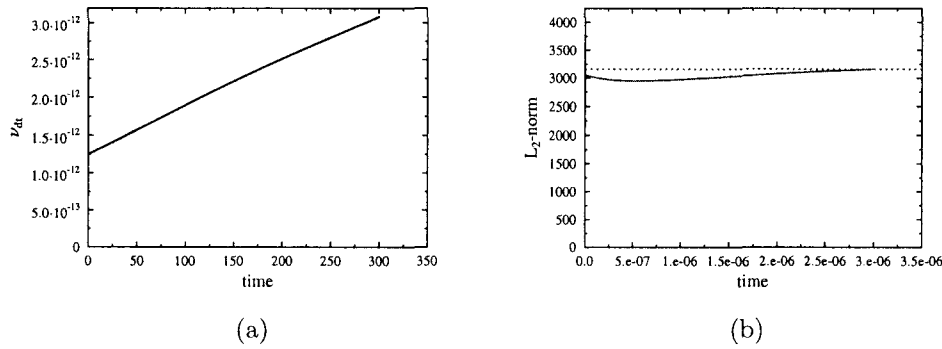


Figure 6.31: (CASE pPL_2) Time histories of (a) the regularization parameter ν_{dt} and (b) (solid line) L_2 norm of the solution using P regulator to control the L_2 norm with $P = 2 \cdot 10^{-16}$, (dotted line) reference level for the L_2 norm.

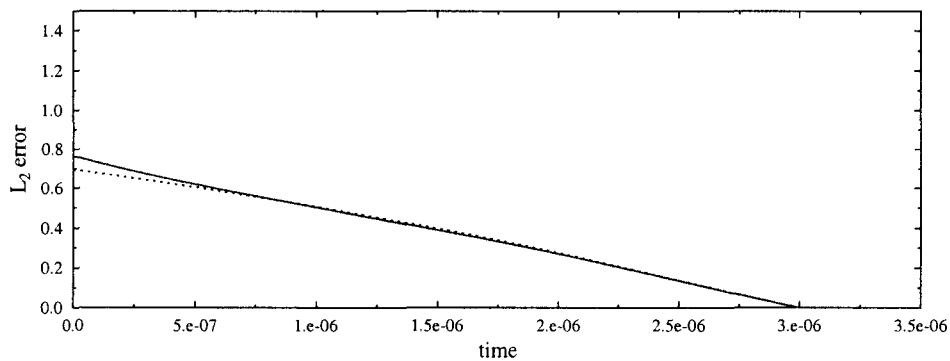


Figure 6.32: (CASE pPL_2) L_2 error norm over the window $[0, T]$, solid line is for the P regulator to control the L_2 norm, dashed line is for a fixed value of ν_{dt}

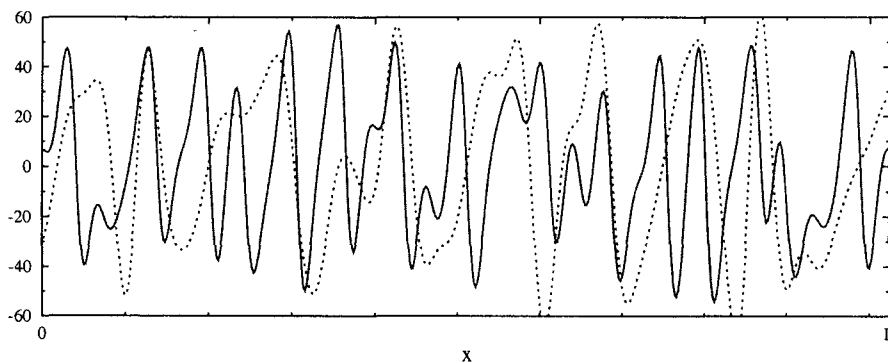


Figure 6.33: (CASE pPL_2) Comparison of the (solid line) the initial condition ϕ in the initial value problem (6.1) and (dashed line) the solution of the regularized terminal value problem (5.5) $p(t = 0)$.

- Here we choose again a starting value from the fixed values already tested. The value used is $3.1 \cdot 10^{-12}$.
- We start by setting K_D to zero and increase K_P until the perturbed system is stable. We are interested in two properties of the algorithm, namely the adjustment time and overshoot. We want the overshoot to be as small as possible. With the PD -regulator we have the possibility of increasing K_P and use K_D to decrease the size of the overshoot. So now the value of K_P will be much larger, five orders of magnitude.
- The K_D parameter is used to control the feedback from the derivative of the error. This parameter will decrease the overshoot and increase the adjustment time. For large values, the perturbed terminal value problem this method is unstable. This will be the last variable we will set and it will be as large as possible to decrease the overshoot and still be stable. K_D is adjusted to make the L_2 norm of the solution to the terminal value problem to be close to the reference level when $t = 0$.

Figure 6.34 is similar to 6.31, but the value of ν_{dt} is slightly smaller for the PD regulator when t is close to zero. This causes the solution of the terminal value problem to have a larger L_2 norm than the solution obtained using the P regulator. Both of the regulators do a good job in keeping the L_2 norm close to the reference level, see figure 6.34 and figure 6.31.

6.2.5 H^{-1} norm with P -regulator

Here we will use the H^{-1} norm as a reference level. This norm is more focused on the large scales of the problem and therefore could be less affected by noise. Generally, it seems that this norm is lagging in time in comparison with the L_2 norm. In figure 6.39 one can see that the solution has retained the large scales properties. However, the solution has more energy because of the time lag present using the H^{-1} norm. If we look at figure 6.37, we can see that the energy starts decreased during the solution to the terminal value problem. It continues to decrease even though the L_2 norm of the solution is higher than the reference level. This follows from that when t is close to T , the H^{-1} norm of the solution to the terminal value problem is small so the P -regulator will try to decrease ν_6 .

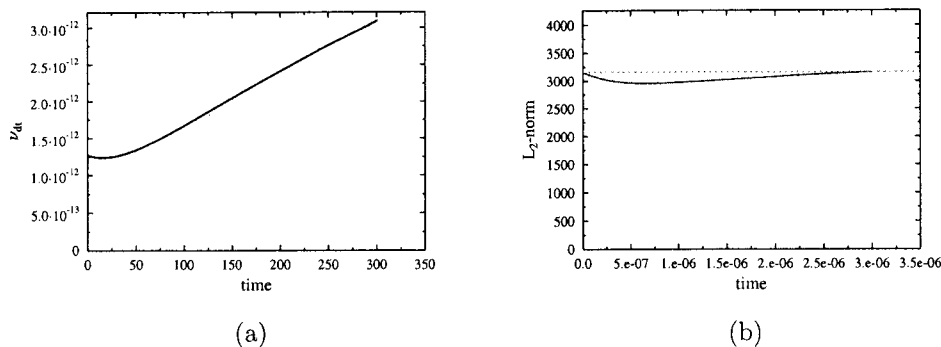


Figure 6.34: (CASE $pPDL_2$) Time histories of (a) the regularization parameter ν_{dt} and (b) (solid line) L_2 norm of the solution using PD regulator to control the L_2 norm with $P = 1 \cdot 10^{-11}$, $D = 7 \cdot 10^{-17}$, (dotted line) reference level for the L_2 norm.

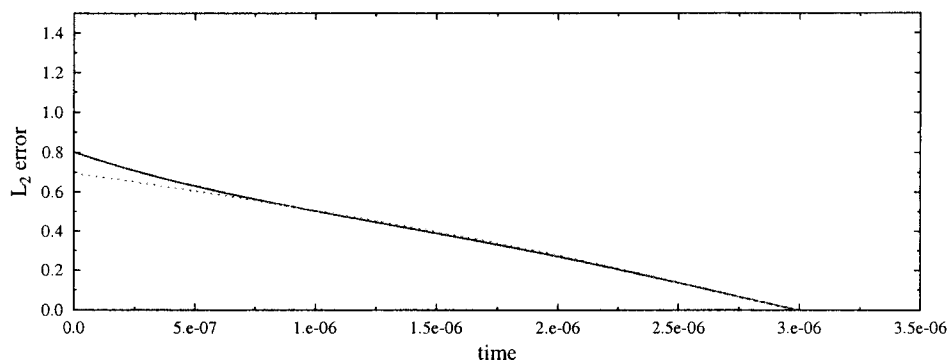


Figure 6.35: (CASE $pPDL_2$) L_2 error norm over the window $[0, T]$, solid line is for the PD regulator to control the L_2 norm, dashed line is for a fixed value of ν_{dt}

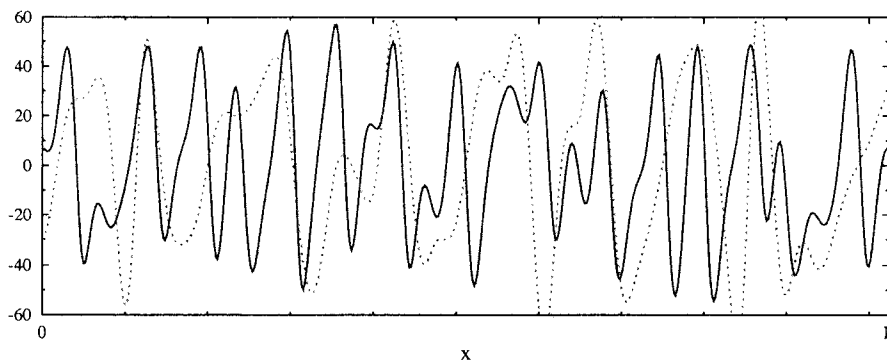


Figure 6.36: (CASE $pPDL_2$) Comparison of the (solid line) the initial condition ϕ in the initial value problem (6.1) and (dashed line) the solution of the regularized terminal value problem (5.5) $p(t = 0)$.

Unfortunately, it decreased the magnitude of the regularization coefficient too much and the solution to the terminal value problem will be given a sudden peak of energy. But here P is again chosen in such a way that this will happen after $t = 0$.

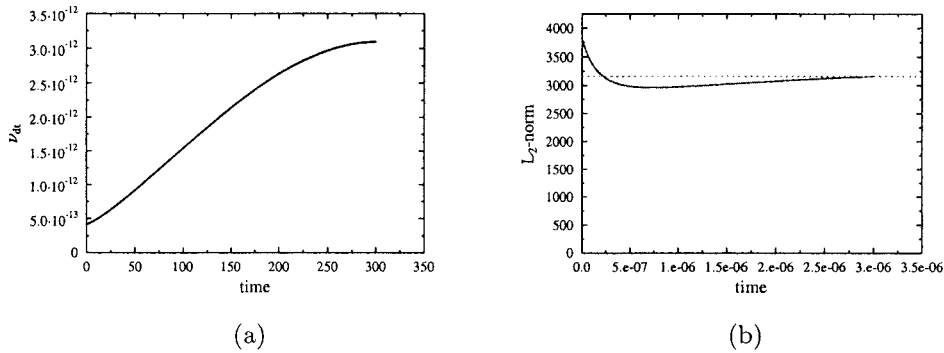


Figure 6.37: (CASE pPH^{-1}) Time histories of (a) the regularization parameter ν_{dt} and (b) (solid line) L_2 norm of the solution using P regulator to control the H^{-1} norm with $P = 4 \cdot 10^{-14}$, (dotted line) reference level for the L_2 norm.

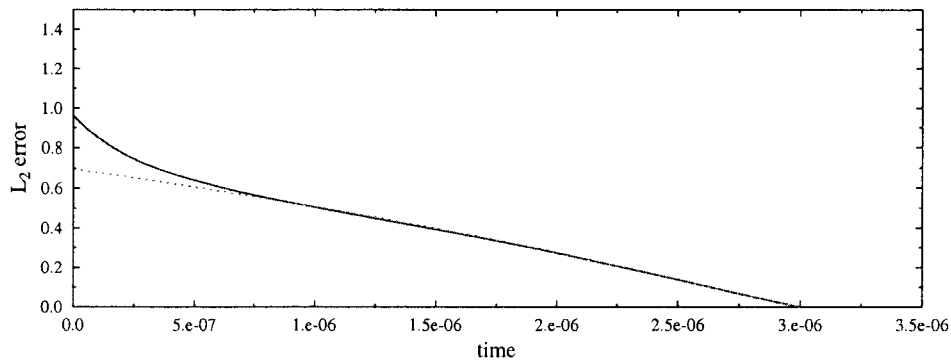


Figure 6.38: (CASE pPH^{-1}) L_2 error norm over the window $[0, T]$, solid line is for the P regulator to control the H norm, dashed line is for a fixed value of ν_{dt}

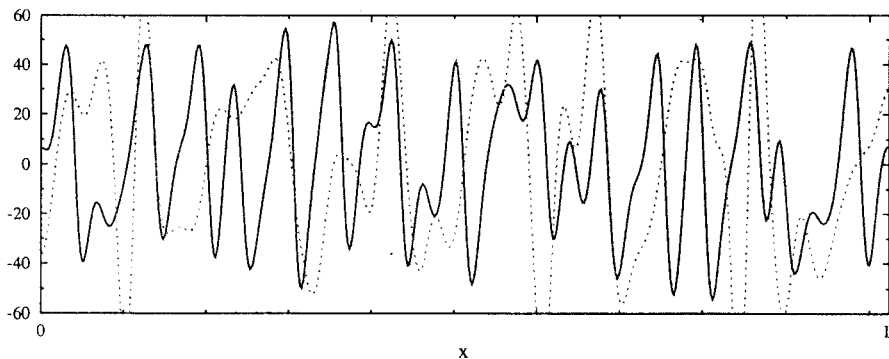


Figure 6.39: (CASE pPH^{-1}) Comparison of the (solid line) the initial condition ϕ in the initial value problem (6.1) and (dashed line) the solution of the regularized terminal value problem (5.5) $p(t = 0)$.

Chapter 7

Conclusions & Summary

In this thesis we have in the first part examined hyperviscous and pseudo-parabolic regularization of the backward Kuramoto–Sivashinsky equation using fixed magnitudes of the regularization coefficients. In the second part of this thesis we proposed a new approach to regularize the terminal value problem of the Kuramoto–Sivashinsky equation. The basic idea is that instead of keeping the amount of regularization constant during the backward solution, we adapt it according to some criteria. We used the L_2 norm and H^{-1} norm and tried to keep one of these norms constant by changing the value of the regularization coefficients ν_6 and ν_{dt} . Three different algorithms were used namely, the P regulator, PD regulator and an instantaneous adaptation based on Newton’s method.

The size of L is related to how accurate we can solve the terminal value problem of the Kuramoto–Sivashinsky equation. A large value of L will make the solutions less accurate. We also compared solutions to the regularized terminal value problem for the Kuramoto–Sivashinsky equation with fixed value of the regularization parameter to solutions of analogous problems, but with the nonlinear term removed. It was found that the linearized problem is more stable and it is possible to get a more accurate solution to this problem than for the full Kuramoto–Sivashinsky equation.

The main findings can be summarized as follows:

- We can see from comparing the figures in section 6.1 and 6.2 that the pseudo-parabolic regularization works better than the hyperviscous regularization. A likely reason is that the change of the energy function spectrum due to regularization is

less significant for the pseudo-parabolic regularization technique than for the hyper-viscous regularization technique.

- When the L_2 norm is used to measure the error in the adaptive schemes tried, i.e., P , PD and the instantaneous adaptation, they all perform worse than a “good” fixed value of the amplitude of the regularization coefficient. However, the L_2 norm is sensitive to shifts in real space. Therefore, even though the error is high in the L_2 norm the solutions obtained with adaptive techniques are often “visually” better than solutions obtained with fixed values of the regularization coefficients; this seems to indicate that for practical purposes the L_2 norm might not be the most appropriate.
- We show that the size of the L_2 error is dependent on the size of the domain L . More specifically, with increasing L we get less accurate solution to the terminal value problem.

In conclusion we believe that the idea of dynamically changing the amount of regularization used is worth pursuing. We would like to have found a method that worked better than using any fixed value. Since regularization of nonlinear PDE is a relatively new topic, we are missing some theoretical background. For example, continuous dependence on the regularization parameter ν or given a time window T and a regularization method what is the least error possible. This and other problems are still unsolved in regularization of nonlinear PDE.

Appendix A

Inertial range in the Navier Stokes equation

In the Navier Stokes equation three assumption are needed to ensure the existence of the inertial range,

- In the inertial sub range all the flux F towards higher wavenumbers is lost through dissipation ε

$$(A.1) \quad F(\kappa) = \int_{\kappa}^{\infty} \hat{w}_{\bar{\kappa}} d\bar{\kappa} = \varepsilon$$

- In the inertial sub range very little energy is being lost. Because of very small dissipation and absence of nonlinear fluxes into the Fourier modes that correspond to the inertial sub range

$$(A.2) \quad \frac{dF}{d\kappa} \cong 0$$

- The flux past any wavenumber in the inertial sub range is of the order

$$(A.3) \quad F(\kappa) \approx \frac{\kappa E(\kappa)}{\tau(\kappa)}$$

where

$$(A.4) \quad \tau(\kappa) = \frac{1}{\sqrt{\kappa^3 E(\kappa)}}$$

is the only characteristic time that can be constructed with the use of κ and $E(\kappa)$ only. The reason we can do this is that the scales are well separated. Or to make it more

clear, the Fourier modes containing most of the energy correspond to wavenumbers that are much smaller than the wavenumbers where most of the dissipation takes place.

Notice that the expression for the flux $F(\kappa)$ past a wavenumber in the inertial sub range comes from dimensional analysis.

Appendix B

Inertial range in the Kuramoto–Sivashinsky equation

In this appendix we want to compare the assumptions needed to ensure the existence of the inertial range in the Navier Stokes equation, cf. Appendix A, with the assumptions needed to ensure the existence of the inertial range in the Kuramoto–Sivashinsky equation. We will need three assumptions and we will show that the argument for a inertial range in the Kuramoto–Sivashinsky equation is weaker than the argument for a inertial range in the Navier Stokes equation.

The first assumption is that in the dissipative scales the energy flux into wavenumber κ is equal to the dissipation at wave-number κ

$$(B.1) \quad \frac{dF(\kappa)}{d\kappa} = -\kappa^4 E(\kappa).$$

This assumption is easy to accept by noting that the Fourier modes corresponding to large wave-number are small or close to zero.

The second assumption is that in the inertial sub range, no energy is lost or gained through injection by the κ^2 operator or dissipated through by the $-\kappa^4$ operator and the flux into the inertial sub range is

$$(B.2) \quad \frac{dF(\kappa)}{d\kappa} = 0.$$

The first part of this assumption is exactly true in only one point $\kappa = 1$, but not in a finite range. Note that this is true for the Navier Stokes equation as well, however in Navier

Stokes the slope is $\kappa^{-5/3}$, whereas in the Kuramoto-Sivashinsky equation the slope is κ^{-4} . We can assume that the Kuramoto-Sivashinsky equation has a power law region of $C\kappa^{-4}$ inside the range $[\kappa_1, \kappa_2]$. This means that the linearized Kuramoto-Sivashinsky equation in Fourier space will look like

$$(B.3) \quad \frac{\partial E}{\partial t} = AC\kappa^4 = \frac{C}{\kappa^2} - C, \quad \kappa \in [\kappa_1, \kappa_2].$$

The first part of the second assumption is that the above expression is independent of changes in κ . This first part of the assumption is very hard to accept. If one does the same for the Navier Stokes equation, assume that there exists a power law region of $C\kappa^{-5/3}$ inside the range $[\kappa_1, \kappa_2]$. This means that the linearized dynamic equation for the energy function spectrum will have the form

$$(B.4) \quad \frac{dE(\kappa)}{dt} = -\kappa^2 C \kappa^{-5/3} = C\kappa^{1/3}, \quad \kappa \in [\kappa_1, \kappa_2].$$

Here one makes the same assumption, but this function clearly has a weaker dependence on κ than the previous one. How the nonlinear term behaves we do not know, so the second part of the second assumption could be valid.

The third and last assumption is that the flux past any wave-number in the inertial range is

$$(B.5) \quad F(\kappa) = \kappa^4 E(\kappa).$$

This is kind of a circular argument. One assumes that the nonlinear function behaves in this fashion and then $E = C\kappa^{-4}$ inside the power law for the energy function spectrum of the Kuramoto-Sivashinsky equation. Let try and assume that the flux past any wave-number in the inertial range is

$$(B.6) \quad F(\kappa) = \kappa^n E(\kappa).$$

This together with assumption number two means that the energy function spectrum is $C\kappa^{-n}$. So we can have a power law region of any power n . In the Navier Stokes equation, see equation A.3, we get the power law based on physical arguments. We do *not* just assume that the flux has a certain property like in B.5.

Bibliography

- [1] J. Hadamard. *Le probleme de Cauchy et les equations aux derivess pertielles hyperboliques*. Hermann, 1932.
- [2] T. Bewley and B. Protas. Retrograde forecasting of multiscale solution. preprint, 2006.
- [3] R. Lattés and J. L. Lions. *The method of quasireversibility, Applications to partial differential equations*. American Elsevier, 1969.
- [4] W. Muniz, H , de Campos Velho, and F. Ramos. A comparision of some inverse methods for estimating the inital condition of the heat equation. *Journal of Computational and Applied Mathematics*, 103, 1999.
- [5] Y. Kuramoto. Diffusion-Induced Chaos in Reaction Systems. *Progress of Theoretical Physics Supplement*, 64:346–367, 1978.
- [6] G. Sivashinsky. Nonlinear analysis of hydrodynamic instability in laminar flames. *Acta Astronaut*, 4, 1977.
- [7] R. Temam. *Infinitedimensional Dynamical Systems in Mechanics and Physics*. Springer, 1997.
- [8] B. Nicolaenko, B. Scheurer, and R. Temam. Some global dynamical properties of the Kuramoto-Sivashinsky equations: Nonlinear stability and attractors. *Physica D Nonlinear Phenomena*, 16:155–183, June 1985.

- [9] I. Kukavica and M. Malcok. Backward behavior of solutions of the Kuramoto-Sivashinsky equation. *Journal of Mathematical Analysis and Applications*, 307:455–464, 2005.
- [10] I. Kukavica. On the behavior of solutions of the Kuramoto-Sivashinsky equation for negative time. *Journal of Mathematical Analysis and Applications*, 166:601–606, 1992.
- [11] R. Peyret. *Spectral Methods for Incompressible Viscous Flow*. Springer, New York, 2002.
- [12] H. Fujisaka and T. Yamada. Theoretical Study of a Chemical Turbulence. *Progress of Theoretical Physics*, 57:734–745, March 1977.
- [13] R. W. Wittenberg and P. Holmes. Scale and space localization in the Kuramoto-Sivashinsky equation. *Chaos*, 9:452–465, June 1999.
- [14] Y. Pomeau, A. Pumir, and P. Pelce. Intrinsic Stochasticity with Many degrees of Freedom. *Journal of Statistical Physics*, 37(1/2), 1984.
- [15] D. Gottlieb and S. A. Orszag. Numerical analysis of spectral methods: Theory and applications. *SIAM*, 28, 1977.
- [16] Matteo Frigo and Steven G. Johnson. The design and implementation of FFTW3. *Proceedings of the IEEE*, 93(2):216–231, 2005. special issue on "Program Generation, Optimization, and Platform Adaptation".
- [17] C. Canuto, M. Y. Hussaini, A. Quarteroni, and T. A. Zang. *Spectral Methods Fundamentals in Single Domains*. Scientific Computation. Springer, 2006.
- [18] S. A. Orzag. Numerical simulation of incompressible flows within simple boundaries I: Glerkin (spectral) representations. *Stud. Appl. Math.*, 50:293–327, 1971.
- [19] T. Bewley. *Numerical Methods in Science and Engineering*. UC San Diego, 2007.

- [20] K. A. Ames and L. E. Payne. Continuous dependence on modeling for some well-posed perturbations of the backward heat equation. *Journal of Inequalities and Applications*, 3(1):51–64, 1999. doi:10.1155/S1025583499000041.
- [21] R. E. Showalter and T. W. Ting. Pseudoparabolic partial differential equations. *SIAM Journal on Mathematical Analysis*, 1(1):1–26, 1970.
- [22] R. E. Showalter. The final value problem for evolution equations. *J. Math. Anal. Appl.*, 47:563–572, 1974.
- [23] R. E. Showalter. Quasi-Reversibility of the first and second order parabolic evolution equations. In A. Carasso and A. P. Stone, editors, *Improperly posed boundary value problems*, Research Notes in Mathematics. Pitman, London 1975.
- [24] Karen A. Ames. On the comparison of solutions of related properly and improperly posed cauchy problems for first order operator equations. *SIAM Journal on Mathematical Analysis*, 13(4):594–606, 1982.
- [25] István Vajk. *State space control*, pages 393–404. CRC Press, 2005.
- [26] W. F. Freiberger, editor. *The International Dictionary of Applied Mathematics*. D. Van Nostrand Company, 1960.
- [27] J H Hyman, B Nicolaenko, and S Zaleski. Order and complexity in the kuramoto-sivashinsky model of weakly turbulent interfaces. *Phys. D*, 23(1-3):265–292, 1986.